

Assessment of the water quality components in turbid estuarine waters based on radiative transfer approximations

LEONID G. SOKOLETSKY,^{a,*} ROSS S. LUNETTA,^a MICHAEL S. WETZ,^{a,#} AND HANS W. PAERL^b

^aU.S. Environmental Protection Agency, National Exposure Research Laboratory, National Research Council, Research Triangle Park, NC 27711, USA

^bUniversity of North Carolina at Chapel Hill, Institute of Marine Sciences, Morehead City, NC 28557, USA

(Received 21 January 2011; accepted in revised form 27 April 2011)

Honoring Anatoly Gitelson on the occasion of his 70th birthday

ABSTRACT

Bio-geo-optical data collected in the Neuse River Estuary, North Carolina, USA were used to develop a semi-empirical optical algorithm for assessing inherent optical properties associated with water quality components (WQCs). Three wavelengths (560, 665, and 709 nm) were explored for algorithm development. WQCs included chlorophyll *a* (Chl), volatile suspended solids (VSS), fixed suspended solids (FSS), total suspended solids (TSS), and absorption of chromophoric dissolved organic matter (a_{CDOM}). The relationships between the measured remote-sensing reflectance and the WQCs were derived based on radiative transfer model calculations. We simulated and analyzed the impact of CDOM absorption in the red and near infrared spectral domains, multiple scattering, and scattering phase function on the accuracy of WQCs prediction. The algorithm was validated by comparing experimental Chl dynamics with predicted values and a numerical comparison between measured and modeled Chl values. The numerical comparison yielded the highest correlation between predicted and measured WQCs for Chl ($R^2 = 0.88$) and the lowest for FSS ($R^2 = 0.00$), while the best and worst mean-normalized root-mean-squares errors were obtained for a_{CDOM} (412.5) and FSS (35% and 59%, respectively). WQCs retrieval accuracy was typically significantly better at values of $a_{TSS,red} > 0.5 \text{ m}^{-1}$.

Keywords: water quality, radiative transfer, estuarine waters

INTRODUCTION

The retrieval of inherent optical properties (IOPs), including absorption (a) and backscattering (b_b) coefficients, from reflectance is a useful conceptual tool for estimating water quality components (WQCs) in natural waters (Cauwer et al., 2004; Dall'Olmo and Gitelson, 2005; Gons, 1999; Ruddick et al., 2001; Peters et al., 2002; Smyth et al., 2006). These WQCs include chlorophyll *a* (Chl), volatile (organic) suspended solids (VSS), fixed (inorganic) suspended solids (FSS), total

suspended solids (TSS), and chromophoric dissolved organic matter (CDOM) absorption (a_{CDOM}). Decomposition from reflectance to IOPs spectra is important because reflectance data may be obtained using either in-situ or remote-sensing (RS) data. IOPs can be directly related to Chl, suspended solids concentrations, and

*Author to whom correspondence should be addressed.
E-mail: sokoletsky.leonid@gmail.com

#Present affiliation: Texas A&M University-Corpus Christi, Department of Life Sciences, Corpus Christi, TX 78412, USA

a_{CDOM} . Thus, reflectance spectra may finally be related with important WQCs and applied to solve various problems in hydrologic optics and hydrologic remote sensing.

In general, reflectance of light measured at the water surface at a single wavelength, cannot be inverted into definite a and b_b since a given reflectance is approximately proportional to the b_b/a ratio. However, a and b_b may be determined using the infrared spectral domain, where absorption by suspended particles is generally negligible (Babin and Stramski, 2002), and the CDOM absorption is estimated from the spectral reflectance measurements. This approach permits expressing a and b_b analytically at other wavelengths from the visual spectrum based on some assumptions concerning the spectral features of these IOPs (Gons, 1999; Ruddick et al., 2001; Peters et al., 2002; Cauwer et al., 2004; Dall'Olmo and Gitelson, 2005).

Both subsurface irradiance reflectance (R) and subsurface remote-sensing reflectance (r_{rs}) are typically used for WQCs analysis. R is defined as a ratio of subsurface upwelling irradiance $E_u(0-)$ to downwelling irradiance at zero depth $E_d(0-)$, and r_{rs} as a ratio of subsurface upwelling radiance $L_u(0-)$ to $E_d(0-)$. Both reflectance types are feasible for application. However, r_{rs} has been utilized more than R because it is assumed that r_{rs} is less dependent on lighting geometry (Morel and Gentily, 1993, 1996; Zaneveld, 1995; Stramska et al., 2000; Højerslev, 2001) and is easily derived from RS measurement data.

For applications involving open ocean waters (Case 1), the decomposition of measured reflectance into IOPs is a relatively simple procedure, due to the small quantity of optically active components and the close relationships between IOPs of water components. However, in inland and coastal (Case 2) waters, the situation is more complex due to the presence of high concentrations of suspended solids and dissolved organic matter that are generally only weakly associated with chlorophyll concentration. In estuarine systems, an intermediate complexity may exist (i.e., partial correlation among WQCs), although some observations yield contradictory results. For example, Yacobi and Gitelson (2000) and Gallegos et al. (2005) found a clear seasonal correlation between Chl and TSS concentrations —especially during spring phytoplankton bloom in Lake Kinneret, Israel, and in the sub-estuary of the Rhode River, Maryland. Vähätalo et al. (2005) obtained good correlation between the spectrally-averaged absorption coefficient of Chl and non-algal particles (NAP) in the North Carolina's Neuse River Estuary (NRE) in fall 2002. Indirect confirmation of similar relationships was also reported for Pamlico Sound (PS) in 2001–2002

(Vähätalo et al., 2005) based on Chl and nephelometric turbidity seasonal intercomparisons. On the other hand, other studies (e.g., Peters et al., 2002; Buzzelli et al., 2003; Gitelson et al., 2007) showed lack of any meaningful relationship of Chl-TSS or Chl-VSS.

The objective of the current study was to develop a semi-empirical optical algorithm using in-situ radiometric measurement data for the assessment of IOPs (a and b_b) and WQCs (Chl, VSS, FSS, TSS, and a_{CDOM}) in support of ocean color satellite monitoring of North Carolina's Albemarle–Pamlico Estuarine System (APES) (Sokoletsky et al., 2011).

MATERIALS AND METHODS

The Neuse River Estuary is the largest tributary of the APES (Fig. 1). This complex is representative of shallow, periodically stratified, semi-lagoonal estuaries, common along the Mid-Atlantic and Gulf of Mexico coasts. The tributary drains some of North Carolina's most productive and rapidly expanding agricultural and urban regions. It originates in the piedmont of North Carolina, near Durham; flows through Raleigh; and empties into PS beyond New Bern (Fig. 1). The Neuse River is approximately 325 km in length, and its depths vary from 2 to 7 m, reaching approximately 7.5 m in the Northern Pamlico basin (Burkholder et al., 2004). The APES supports approximately 80% of commercially and recreationally-caught coastal fisheries species in the Southeastern Atlantic Region (Copeland and Gray, 1991). Over the past several decades, this system has been adversely affected by human activities (i.e., changes in nutrient loadings and habitat degradation) and climatic perturbations. These factors have led to degradation of water/habitat quality, and have caused declines of fisheries resources and of overall ecological condition (Paerl et al., 1998, 2006).

Radiometric measurements

We developed a semi-theoretical underwater optical algorithm for WQCs retrieval in the region of NRE and PS, using surface radiometric data and radiative transfer approximations. The ultimate goal was to incorporate this algorithm into a more general algorithm to be applied for satellite water quality monitoring (Sokoletsky et al., 2011). The Neuse River Estuary Modeling and Monitoring Project (ModMon) was adopted to include radiometric data collections using a Satlantic Hyper Pro profiling instrument. The modified protocols from ModMon were used to collect radiometric data as well as turbidity, Chl, CDOM, VSS, FSS, TSS, diffuse attenuation coefficient, temperature, and salinity data at ten stations for nine dates within the period of years

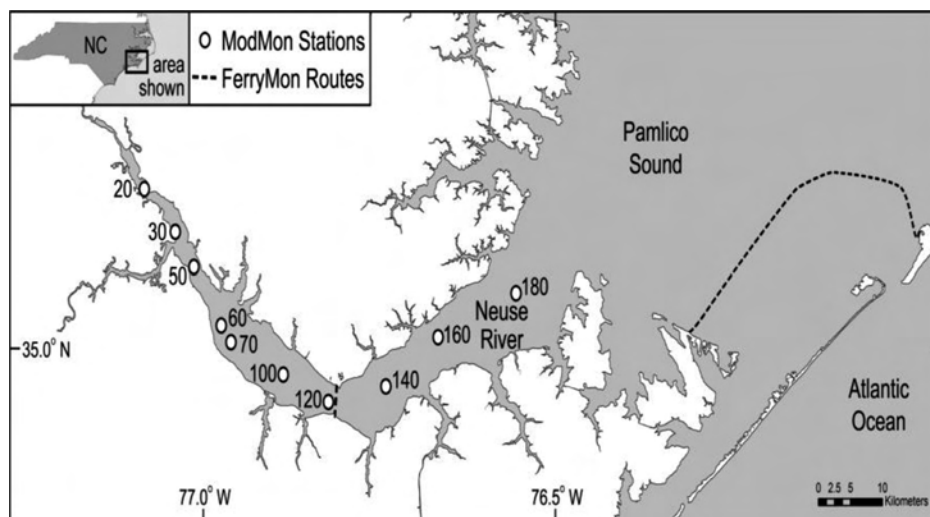


Fig. 1. The Neuse River-Pamlico Sound Estuarine System with ModMon stations and FerryMon routes.

2006–2008 (Fig. 1). All radiometric measurements were captured in morning hours, at zero nadir viewing angles. These measurements included spectra from approximately 350–800 nm with a mean step of 3.3 nm, of both downwelling irradiance just above the water $E_s(\lambda)$ and underwater upwelling radiance $L_u(z, \lambda)$ at depth z .

ProSoft software was used in the processing of $E_s(\lambda)$ and $L_u(\lambda)$ spectra. The values of $L_u(z, \lambda)$ at depths z closest to the surface (0.2–0.5 m) were used in the operational algorithm to simulate the upwelling radiance spectra just below the surface $L_u(0-, \lambda)$. The rationale for this method is based on the concept that the $b_b(0-, \lambda)/a(0-, \lambda)$ ratio is the major factor defining the spectral subsurface reflectance (Gordon et al., 1988; Morel and Gentili, 1993; Kirk, 1994; Jerome et al., 1996; Lee et al., 1998, 2004; Aas and Højerslev, 1999; Forget, 2000; Albert and Gege, 2006; Craig et al., 2006). In turn, in the first approximation, $b_b(z)$ is covariant (proportional) to the $a(z)$ for different types of natural waters (Morel, 1988; Gordon, 1992; Morel and Maritorena, 2001; Sokoletsky, 2003, Ch. 2.2). Thus, the $r_{rs}(z, \lambda)$ may be considered as an optical property weakly-varied with a depth (Gordon and Brown, 1975; Gordon et al., 1975; Kirk, 1981; Morel, 1988; Boynton and Gordon, 2000). Additionally, our measurements and calculations did not show large variations in the observed ratio of $r_{rs}(z, 709 \text{ nm})/r_{rs}(z, 665 \text{ nm})$ at $z < 1 \text{ m}$.

A conversion from the $L_u(0-, \lambda)$ spectra to water-leaving radiance $L_w(\lambda)$ spectra was made by compensating for Fresnel's reflectance ρ_{Fr} of the surface as it is seen from underwater (Mobley, 1999). Because all upwelling radiance measurements were made at nadir (i.e., $\theta_2 = 0^\circ$), Fresnel's reflectance was $\rho_{Fr} = 0.021(\pm 0.001)$. $L_w(\lambda)$ was calculated by (Mobley, 1999):

$$L_w(\lambda) = \frac{1 - \rho_{Fr}}{n_w^2} L_u(0-, \lambda) \quad (1)$$

where n_w is the real part of the refractive index of the water, calculated by the three-term (temperature, salinity, and wavelength) nonlinear model by Quan and Fry (1995), following ancillary measurements in the NRE. For the visible spectrum extremes ($\lambda = 400$ and $\lambda = 700$ nm) the following average values of refractive indices and $L_w(\lambda)/L_u(0-, \lambda)$ were obtained: $n_w(400) = 1.345(\pm 0.001)$, $n_w(700) = 1.332(\pm 0.001)$, $L_w(400)/L_u(0-, 400) = 0.497(\pm 0.001)$, and $L_w(700)/L_u(0-, 700) = 0.506(\pm 0.001)$. Further conversion from the above-water remote-sensing reflectance spectra $R_{rs}(\lambda) = L_w(\lambda)/E_s(\lambda)$ to under-water remote-sensing reflectance spectra $r_{rs}(\lambda) = L_u(0-, \lambda)/E_d(0-, \lambda)$ was realized by the equation derived by Craig et al. (2006) from the radiative transfer simulations:

$$r_{rs}(\lambda) = \frac{R_{rs}(\lambda)}{0.52 + 1.7R_{rs}(\lambda)} \quad (2)$$

The $r_{rs}(\lambda)$ spectra obtained for the NRE indicate that the three local optima were centered in the green [569; 600] nm (first maximum), red [650; 676] nm (total minimum) and near infrared [683; 710] nm (second maximum) spectral ranges (Fig. 2). Figure 2 also illustrates the link between spectral signature profiles for bands 5, 7, and 9 of the MERIS sensor on board the ENVISAT satellite and local $r_{rs}(\lambda)$ optima.

Water quality measurements

ModMon water quality collections included Secchi depth and vertical profiles of geophysical (VSS, FSS,

TSS, fluorescence, temperature, and salinity), chemical (pH, dissolved oxygen, and nutrients), optical ($a_{CDOM}(\lambda)$, turbidity and photosynthetically active radiation—PAR), and biological (size-fractionated pigments, phytoplankton and zooplankton biomass) parameters. Profiles of PAR, temperature, salinity, dissolved oxygen, chlorophyll fluorescence, turbidity, and pH were acquired at 0.5 m intervals at each sampling location. To support underwater optical model development, only subsurface values of WQCs were collected. The ModMon samples for suspended solids ($n = 68$) and both Chl and a_{CDOM} ($n = 79$) were used to support the project.

Chl was determined fluorometrically according to Welshmeyer (1994). VSS, FSS, and TSS were determined using standard methods where samples were filtered using GF/F filters (0.7 μm) (Eaton et al., 2005). Filters were weighed prior and subsequent to filtration, then dried for at least one hour at approximately 105 °C and weighed again for TSS determination. To remove VSS, filters were then ignited at 550 °C in a muffle furnace for 15 min. After drying in a desiccator, filters were weighed to determine the fraction of material remaining, that is, FSS. VSS was then determined by subtracting FSS from TSS.

VSS and TSS estimates can be influenced by the presence of picoplankton because some cells (0.2–2 μm) can pass through the filter. However, ModMon observations used in this study did not usually coincide with summer picoplankton bloom. Only one set of observations (July 22, 2008) was performed in summer. However, our observations have shown that a maximum contribution of picoplankton cell concentration to VSS and TSS was 0.7% and 0.5%, respectively. Thus, VSS contents were assumed to have been comprised primar-

ily of particles of organic origin and phytoplankton cells with sizes $>0.7 \mu\text{m}$, while FSS contents were assumed to be particles of inorganic origin.

A modified Vähätalo et al. (2005) method was used to determine the a_{CDOM} . Absorbance (optical density) spectra of GF/F filtrate samples were analyzed on a Shimadzu UV-1700 PharmaSpec spectrophotometer with Nanopure water as a reference (200–800 nm).

Chl measurements

An additional dataset of surface Chl measurements was obtained through the North Carolina FerryMon Program (Buzzelli et al., 2003). FerryMon consists of two NC Department of Transportation ferries, one traversing the NRE and one traversing the PS. Both ferries were equipped with automated water quality monitoring systems, including a flow-through YSI 6600 sondes that measured chlorophyll fluorescence, conductivity, turbidity, temperature, salinity, dissolved oxygen, and pH (Buzzelli et al., 2003). In-vivo fluorescence was converted to Chl concentrations according to calibration equations relating fluorescence to various concentrations of extracted Chl. The NRE ferry completed 40 crossings per day between Cherry Point and Minnesott Beach, while the PS ferry completed only four crossings daily between Cedar Island and Ocracoke Island (Fig. 1). Surface Chl concentration dynamics in the NRE and PS derived from the ferries data is shown in Fig. 3a–c for 2006–2009.

Optical background

A relationship between the measured R or r_{rs} spectra and IOPs using a simple linear function has been proposed by numerous researchers (Morel and Prieur, 1977; Aas,

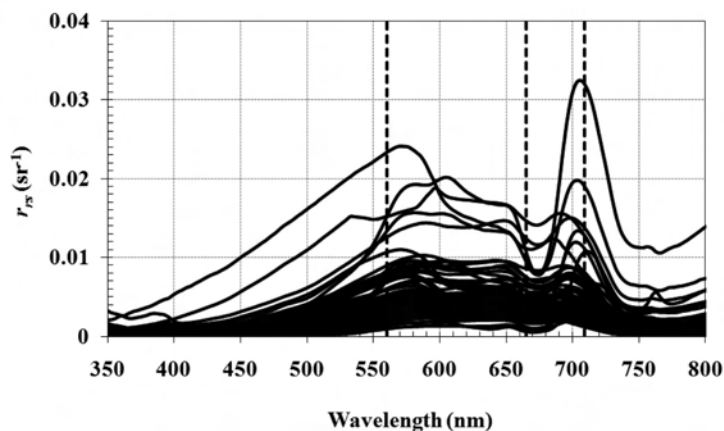


Fig. 2. Remote-sensing reflectance spectra $r_{rs}(\lambda)$ observed in the Neuse River Estuary (NRE) in October 2006 through October 2008. Note the vertical dashed lines corresponding to available MERIS bands: 5th (560 nm), 7th (665 nm) and 9th (709 nm) which are closely aligned to the local $r_{rs}(\lambda)$ optima.

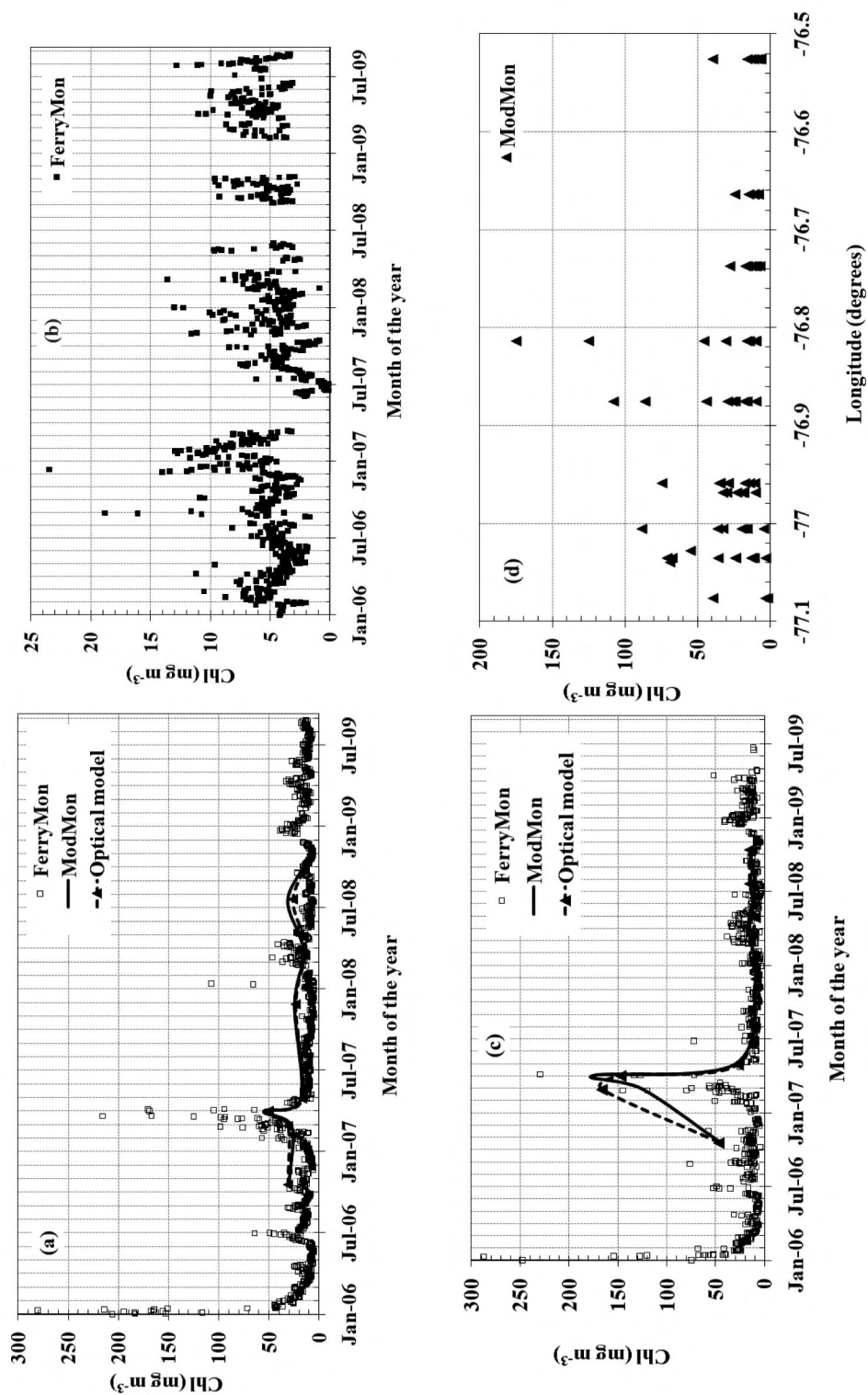


Fig. 3. Temporal (a–c) and spatial (d) Chl variability in NRE (a, c, d) and PS (b) in 2006–2009 derived from the ModMon (a, c, d) and FerryMon (a, b, c) data collections. The data from the 10 ModMon stations were used for plotting (a) and (d), while the data from the only middle river station #120 were used for plotting (c). Daily-averaged Chl values were used for (a) and (b). The results of our underwater optical model are also shown in (a) and (c).

1987; Kirk, 1991, 1994; Morel and Gentili, 1993; Aas and Høgerslev, 1999; Stramska et al., 2000; Smyth et al., 2006) in the general form:

$$R(\mu_1, \lambda) \text{ or } r_{rs}(\mu_1, \mu_2, \lambda) = A * F * [b_b(\lambda)/a(\lambda)] \quad (3)$$

where A is a constant and F is any function of cosine (μ_1) of the solar zenith angle (θ_1) after refraction on the air-water surface, and (only for the case of r_{rs}) of cosine (μ_2) of the viewing nadir angle (θ_2) just below the surface. From eq 3 follows that for any spectral values λ_1 and λ_2 the following equalities are maintained:

$$\frac{R(\lambda_1)}{R(\lambda_2)} = \frac{r_{rs}(\lambda_1)}{r_{rs}(\lambda_2)} = \frac{b_b(\lambda_1)/a(\lambda_1)}{b_b(\lambda_2)/a(\lambda_2)} \approx \frac{G(\lambda_1)}{G(\lambda_2)} \quad (4)$$

where $G = b_b/(b_b + a)$ is termed the Gordon's parameter. For most open waters a condition $b_b \ll a$ is fulfilled. However, in turbid coastal and inland waters with significant particulate matter, backscattering may often be compared with absorption and the term b_b/a should be substituted by G .

Historically, eq 3 has been derived from the quasi-single-scattering approximation (QSSA) that was first proposed by Gordon (1973) for reflectance factor (RF) as follows:

$$RF(\theta_1, \theta_2, \varphi) = \frac{1}{4} \frac{G}{B} \frac{p(\theta)}{\mu_1 + \mu_2}, \quad \frac{1}{2} \int_0^\pi p(\theta) \sin \theta d\theta = 1, \quad (5)$$

where φ and θ are the relative azimuth and scattering angles (all angles are in the water), respectively; $p(\theta)$ is the scattering phase function; B is the backscattering probability, completely determined from the $p(\theta)$ as

$$B = \frac{1}{2} \int_{\pi/2}^\pi p(\theta) \sin \theta d\theta \quad (6)$$

and angle θ is connected with other angles through the geometrical relationship

$$\cos \theta = \mu_1 \mu_2 + \cos \varphi \sqrt{(1 - \mu_1^2)(1 - \mu_2^2)}, \quad (7)$$

where the Z -axis for depths is oriented toward zenith for both in- and out-coming light beams or, alternatively, toward nadir.

An important condition for the application of QSSA is that $p(\theta)$ should be highly peaked in the initial direction of light beam propagation, thus the majority of the scattered light remains in the beam, with losses attributable to absorption and backscattering. A second, and maybe more notable, assumption is that the probability of photon absorption is great. Further simplification of QSSA may be obtained by exploring $p(\theta)$ with the constant scattering in backward hemisphere (at scattering

angles from $\pi/2$ to π). In this case, from eq 6 it follows that $p(\theta) = 2B$. The result of this substitution into eq 5 is:

$$RF(\theta_1, \theta_2) = \frac{1}{2} \frac{G}{\mu_1 + \mu_2}, \quad (5')$$

Eq 5' is not exact, because phase functions typically exhibit small features in the backward hemisphere. However, this equation provides an initial insight into the problem. The underlying conditions for the application of QSSA are typically met only for Case 1 waters, where phytoplankton cells are the main factor modifying optical properties and the contribution of total scattering to total attenuation is low. In more complex estuarine waters, other components may introduce a large multiple-scattering light contribution into backscattered light, potentially leading to serious deviations from QSSA. For simplicity, a single-scattering albedo $\omega_0 = b/c$ (b and c are scattering and attenuation coefficients, respectively) is commonly used to determine the relative contribution of scattering to the total attenuation.

QSSA validation for selected scattering phase functions has demonstrated (Gordon, 1973) that for clear oceanic waters, relative errors were within 0.5% for $\omega_0 \leq 0.6$, and about 12% for $\omega_0 \leq 0.85$. Similar results were obtained by Anikonov and Ermolaev (1977) and by Levin (1998) for several selected scattering phase functions. However, much higher QSSA errors were reported by Kokhanovsky and Sokoletsky (2006b). They validated QSSA for RF and for hemispherical reflectance (plane albedo, PA) by comparing QSSA with Mishchenko's invariant imbedding method, IIM (Mishchenko et al., 1999). Five different phase functions representing a wide range of scattering media — from weakly anisotropic (with asymmetry parameter $g = 0.50$) to strongly anisotropic (with $g = 0.96$) — were used for computations. Results indicated that for clear waters (simulated by $g = 0.50$ and $g = 0.70$ at $\omega_0 \leq 0.7$) at solar zenith angles $\theta_0 \in [17^\circ; 70^\circ]$, relative errors were $\delta \in [-45\%; -28\%]$ and $\delta \in [-35\%; -12\%]$ for RF and PA, respectively. For turbid waters (simulated by $g = 0.91$ and $g = 0.96$ at $\omega_0 \leq 0.99$) at the same range of θ_0 , errors were even higher: $\delta \in [-64\%; -43\%]$ and $\delta \in [-44\%; -32\%]$ for RF and PA, respectively.

Similar results for RF and PA were obtained by Sokoletsky and Kokhanovsky (2005). The QSSA approximation yielded relative error of PA and spherical albedo (SA) $< 24\%$ and $< 2.5\%$, respectively, at $\omega_0 \leq 0.9$ independently on the selected phase function, but errors sharply increased at larger values of ω_0 (Sokoletsky and Kokhanovsky, 2005). Thus, errors associated with QSSA application for water bodies may be more signifi-

cant than assumed in earlier studies.

Gordon and his co-workers have extended a QSSA for R (Gordon et al., 1975) and for r_{rs} (Gordon et al., 1988). The r_{rs} has been approximated by the quadratic function of G (Gordon et al., 1988, their eq 2):

$$r_{rs} = G(0.0949 + 0.0794G). \quad (8)$$

Table 1 lists the analytical expressions for r_{rs} derived by different authors for optically deep waters. The values of $G = G_{max}$ and $r_{rs}(G_{max})$ for each expression, at which a deviation of r_{rs} versus G from linear dependency is still <5%, are also presented in the Table 1 and Fig. 4. Only positive, physically relevant, values of G were considered for dependences. Calculations indicated that all the above-mentioned relationships r_{rs} vs. G may be assumed linear for small values of $G < G_{max} = 0.041 \pm 0.027$.

To increase the accuracy in reflectance spectra decomposition into IOPs, some authors have incorporated simulated parameter values provided in look-up tables (LUTs) that include wavelengths, solar zenith and sensor viewing angles, absorption and scattering coeffi-

cients, Chl concentration, and molecular scattering and backscattering contributions to the total scattering and backscattering, respectively (Morel and Gentili, 1993; Morel et al., 2002). IOPs or Chl may be estimated by interpolation using the LUTs. However, as it was noted by Lee et al. (2004), the limited number of parameter values and non-linear dependencies between them render this procedure inaccurate and poorly suited for algorithm development.

Another widely used approach incorporates spectral reflectance ratios. This approach largely removes geometrical factors and bottom influence effects from the solution, and flattens the non-linear behavior of reflectance as a function of IOPs. We used a simulation of a spectrally derived Gordon's parameter ratio instead of a spectral reflectance ratio to demonstrate improvements in the accuracy associated with the use of this approach.

The measured reflectance (e.g., R and r_{rs}) of the water illuminated by natural light can be represented as a superposition of reflectances (RF, PA and SA). This permits the expression of reflectance via IOPs and angular

Table 1

Approximations for the remote-sensing reflectance of optically deep water. G_{max} is defined as the upper boundary of G values at which deviations of dependence $r_{rs}(G)$ from linearity are smaller than 5% (only positive values of r_{rs} were considered). Designations: $G' = G/(1-G)$; NRMSE is the normalized (to the mean IIM value) root-mean-squares error between the given approximation and numerically (IIM) calculated r_{rs} ; NRMSE is the normalized (to the mean of all considered values) root-mean-squares difference between the given approximation and the approximation expressed by eq 21, Case 2 waters. All calculations were performed for the following ranges of parameters: $\theta_0 \in [0^\circ; 61.7^\circ]$, $\theta_2 = 0^\circ$, $\lambda = \{560 \text{ nm}, 665 \text{ nm}, 709 \text{ nm}\}$, $\omega_0 \in [0.1; 0.99]$

Approximation	G_{max}	$r_{rs}(G_{max})$	NRMSE %	NRMSE %	References
$r_{rs} = G(0.0949 + 0.0794G)$	0.060	0.0060	35.2	32.9	Gordon et al. (1988), eq 2
$r_{rs} = 0.0922G'$	0.048	0.0046	50.2	23.3	Morel and Gentili (1993), eq 13
$r_{rs} = 0.083G'$	0.048	0.0042	33.4	20.5	Kirk (1994), eq 6.5
$r_{rs} = -0.00042 + 0.112G' - 0.0455(G')^2$	0.048	$0.050F_1(\mu_0)$	54.5	25.9	Aas and Højerslev (1999), eq 27
$r_{rs} = F_1(\mu_0)G'$, $F_1(\mu_*) = \frac{0.45 - 0.12\mu_*}{5.20 - 1.82\mu_*}$	0.098	0.0112	68.8	41.8	Jerome et al. (1996), eq 4
$r_{rs} = G(0.070 + 0.155G^{0.752})$	0.006	0.0005	14.1	13.4	Lee et al. (1998), eq 16
$r_{rs} = G(0.084 + 0.170G)$	0.025	0.0022	13.8	11.2	Lee et al. (1999), eq 4
$r_{rs} = G(0.085 + 0.208G^{1.193})$	0.038	0.0034	21.0	13.1	Forget (2000), eq 6
$r_{rs} = 0.197G[1 - 0.636 \exp(-2.552G)]$	0.011	0.0009	15.2	12.3	Lee et al. (2004), eq 8
$r_{rs} = 0.0512G(1 + 4.6659G - 7.8387G^2 + 5.4571G^3) F_2(\mu_1, \mu_2)$, $F_2(\mu_1, \mu_2) = (1 + 0.1098/\mu_1)(1 + 0.4021/\mu_2)$	0.011	$0.00059F_2(\mu_1, \mu_2)$	9.2	7.1	Albert and Gege (2006), eq 3.11
$r_{rs} = G(0.0895 + 0.1247G)$	0.036	0.0034	19.1	19.4	Craig et al. (2006), eq A3
$r_{rs} = 0.2874G(1 + 0.2821G - 1.019\mu_1 + 0.4561\mu_1^2)$	0.078–0.087	0.0102–0.0130	2.1	0.0	Current study, eq 21, Case 2 waters

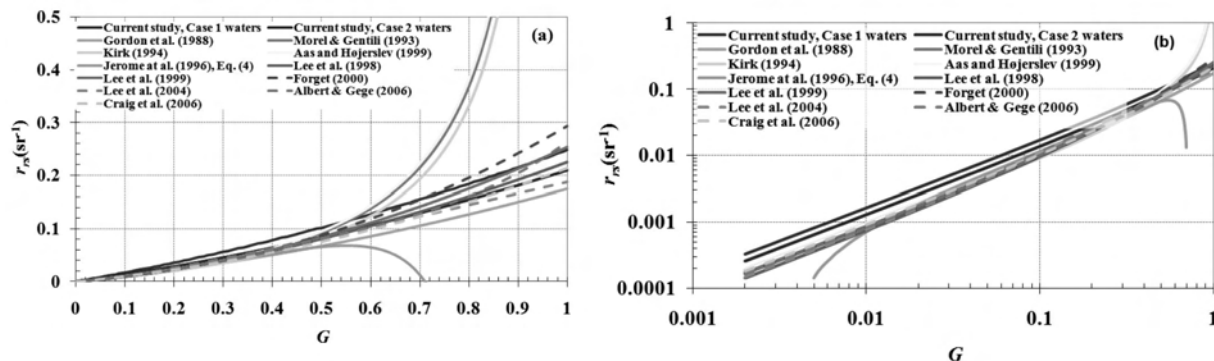


Fig. 4. Relationships between subsurface remote-sensing reflectance r_{rs} and Gordon's parameter G plotted according to the current study (eq 21) and other approximations found in the literature using both linear (a) and logarithmic (b) scales. Cosine of the solar zenith angle and cosine of the nadir viewing angle were accepted to be 0.925 and 1, respectively.

characteristics. Some examples of the expressions for R using PA and SA can be found in the literature (Gordon, 1976; Morel and Gentili, 1991; Haltrin, 1998a; Højerslev, 2004; Sokoletsky, 2004, 2005; Sokoletsky and Gallegos, 2010). The expression for r_{rs} using RF and SA will be derived in the "Modeling remote-sensing reflectance" sub-section of the current study.

RESULTS

Chlorophyll measurements

NRE Chl values illustrated in Fig. 3a,c,d were nearly always greater than in the PS (Fig. 3b) and both were highly variable (NRE: 0.11–645 mg m⁻³ and PS: 0.11–84 mg m⁻³). Mean observed values were significantly greater for the NRE (15.1 ± 25.7 mg m⁻³; $n = 142,265$) than the PS (4.4 ± 3.3 mg m⁻³; $n = 173,918$). There were periods when Chl stably exceeded 40 mg m⁻³ in the NRE for several successive days (Fig. 3a). This Chl threshold value is especially important because it corresponds to the Total Maximum Daily Load (TMDL) established for the NRE (Borsuk et al., 2003). Variability in concentration generally increased with distance from the oceanic outer banks to the NRE (Fig. 3d). An overall comparison of the FerryMon and ModMon measurements (Fig. 3a), does not indicate an apparent agreement between datasets. However, a correspondence is evident between ModMon Chl data collected from the NRE central station #120 (N34.95° W76.81°) and the Chl data from the FerryMon sampling sites located within 200 m distance from this station (Fig. 3c). Additionally, the substantial phytoplankton bloom that occurred between March and April 2007 was observed during both programs (Fig. 3c).

Optical classification of the APES

We utilized the profile data to characterize various WQC parameters and to examine potential relationships between constituents. Figure 5 demonstrates a relatively good correlation between Chl and VSS and TSS, and poor correlation between Chl and FSS and $a_{CDOM}(412.5$ nm). As previously mentioned, observations in the NRE by Vähätalo et al. (2005) and in the PS by Buzzelli et al. (2003) also indicated a good correlation between Chl and TSS and poor correlation between Chl and $a_{CDOM}(\lambda)$. Accordingly, the APES represents a water body of intermediate complexity between Case 1 and Case 2 waters (Morel, 1988; Mobley et al., 2004).

A spectral analysis of $r_{rs}(\lambda)$ shows that a ratio of the second maximum to the global minimum is strongly dependent on concentration of Chl, VSS, and TSS (Fig. 6). These relationships provided support for the application of near infrared to red ratios for WQCs retrieval. Another important observation is the typical inverse dependence of the $r_{rs}(\lambda)$ ratio of the first maximum to the global minimum on a_{CDOM} , although this dependence was not true for all samples (Fig. 7).

The bottom depths Z and the spectral diffuse attenuation coefficient K_d in the region of the NRE were measured recently at fixed study stations shown in Fig. 2 (Paerl et al., 2001; Vähätalo et al., 2005). The minimal values of these parameters were 4.0 m and 1.0 m⁻¹ for Z and K_d , respectively. Thus, minimal values of optical depths, calculated as ZK_d , have been estimated as equal to 4.0 for the NRE. This allowed us to consider the NRE water layers as semi-infinite—effectively neglecting the influence of bottom reflectance on upwelling radiance and resultant surface reflectance (Gordon and Brown, 1974; Sokoletsky, 2005; Sokoletsky et al., 2009).

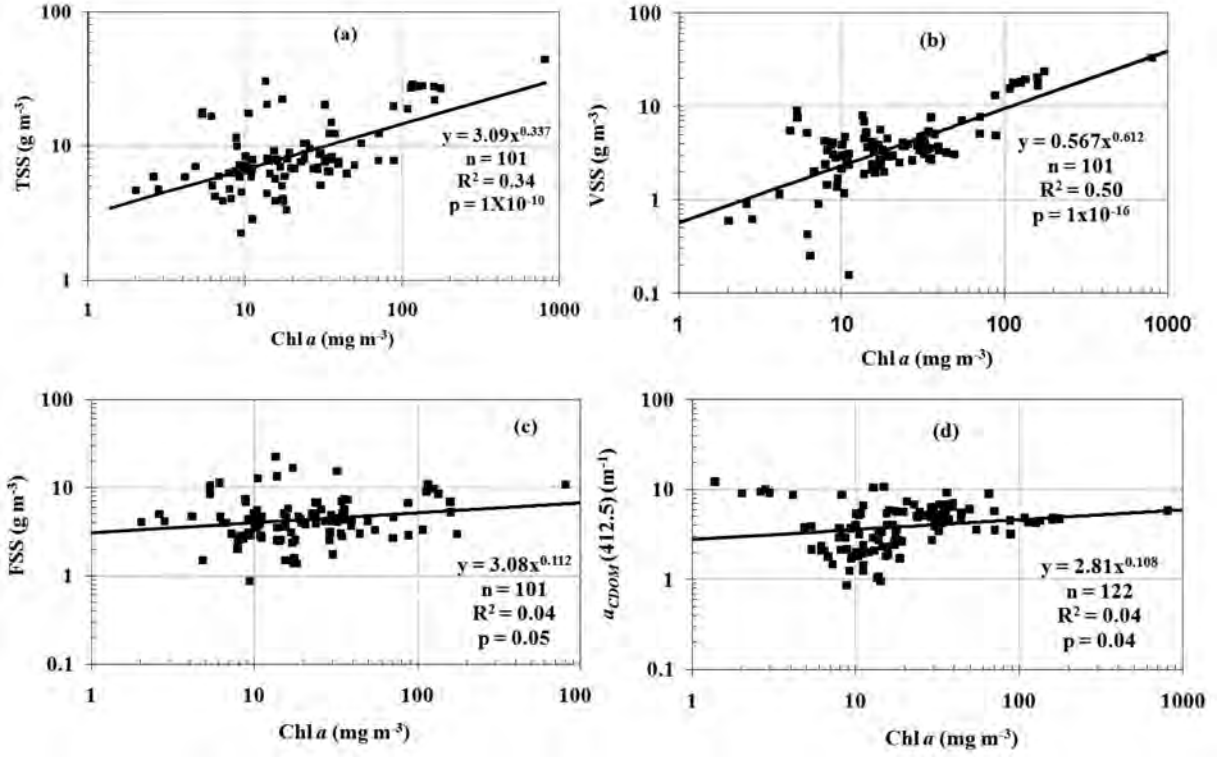


Fig. 5. Relationships among water quality components in the NRE (2006–2008). A relatively good correlation between Chl and TSS (a) and VSS (b), and a poor correlation between Chl and FSS (c) and $a_{CDOM}(412.5)$ (d) indicated intermediate water conditions (Case 1–2). Power curve and associated statistics were used to obtain the best fit.

Modeling remote-sensing reflectance

Below is a derivation of the subsurface optical model for remote-sensing reflectance, $r_{rs}(\lambda)$, of the surface illuminated by natural light. This optical property may be presented (wavelength dependence omitted for simplicity), as the fraction

$$r_{rs} = \frac{L_u^{dir} + L_u^{diff}}{E_d^{dir} + E_d^{diff}}, \quad (9)$$

where E_d^{dir} and E_d^{diff} are the direct and the diffuse parts of the downwelling irradiance, respectively, L_u^{dir} and L_u^{diff} are the direct and the diffuse parts of the upwelling radiance. Eq 9 is equivalent to eq 10

$$r_{rs} = (1 - d_E) \frac{L_u^{dir}}{E_d^{dir}} + d_E \frac{L_u^{diff}}{E_d^{diff}}, \quad (10)$$

where

$$d_E = \frac{E_d^{diff}}{E_d^{diff} + E_d^{dir}} \quad (11)$$

is the diffuse part of the total irradiance incoming just below the water surface. Taking into account definitions

of RF and SA (Nicodemus, 1965; van de Hulst, 1980; Hapke 1993; Otremba, 2003; Zhang and Voss, 2005; Kokhanovsky and Sokoletsky, 2006a), we can rewrite eq 10 in the following form

$$r_{rs} = \frac{1}{\pi} [(1 - d_E)RF + d_E SA], \quad (12)$$

Note, that irradiance reflectance may be similarly presented as a superposition of PA and SA (Haltrin, 1998a; Sokoletsky, 2004, 2005; Sokoletsky and Gallegos, 2010). An expression by Højerslev (2001) has been used for calculation of d_E :

$$d_E(\lambda, \theta_0) = 0.3735 + 4.15 \times 10^{-3}(\theta_0 - 40) + 1.095 \times 10^{-4}(\theta_0 - 40)^2 + 1.1 \times 10^{-6}(\theta_0 - 40)^3 + [-80 \times 10^{-4}(\lambda - 500) + 2.0 \times 10^{-6}(\lambda - 500)^2] \times [1 + 3.0 \times 10^{-3}(\theta_0 - 40)] \quad (13)$$

where wavelength λ and the solar zenith angle θ_0 are expressed in nanometers and degrees, respectively. This expression was derived using an average value for two maritime atmospheres (10 and 30 km visibilities), and was

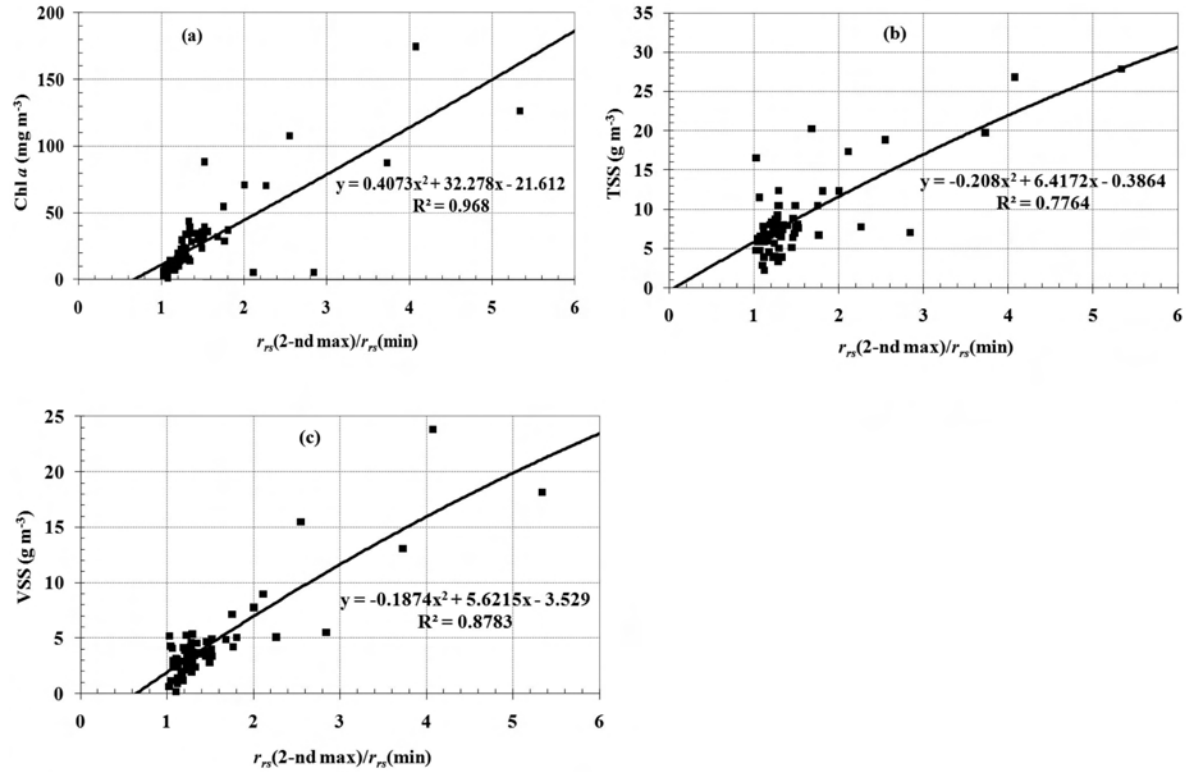


Fig. 6. Relationships between the $r_{rs}(\lambda)$ ratio of second maximum to the global minimum and Chl (a), TSS (b), and VSS (c) concentrations. Polynomial curves were used to obtain the best fit.

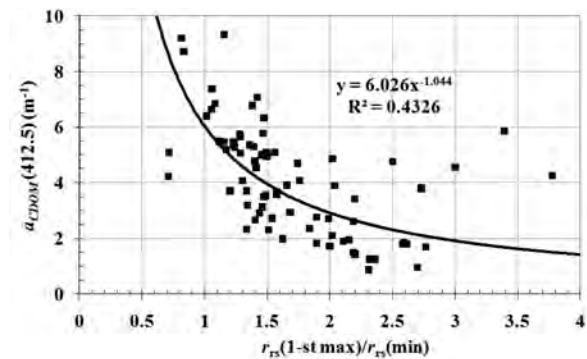


Fig. 7. Relationships between the $r_{rs}(\lambda)$ ratio of first maximum to the $r_{rs}(\lambda)$ global minimum and $a_{CDOM}(412.5 \text{ nm})$. Power curve was used to obtain the best fit.

considered to be a reliable approximation for the APES.

A calculation of θ_0 was carried out using the standard astronomical formulae (Exell, 1981; Duffie and Beckman, 2006) with the equation of time (EqT, in minutes) derived from Helyar (2001) in the form:

$$\begin{aligned} \text{EqT} = & -0.025 + 0.4079\cos(T) - 7.394\sin(T) \\ & - 3.297\cos(2T) - 9.359\sin(2T) - 0.1371\cos(3T) \\ & - 0.2365\sin(3T) - 0.1588\cos(4T) - 0.1604\sin(4T) \end{aligned} \quad (14)$$

where T is parameter depending on the date of the Julian day (N_d):

$$T = 2\pi(N_d - 1)/366. \quad (15)$$

A relationship between the cosines of incoming (μ_0) and refracted (μ_1) angles follows from the Snell's law used in the form:

$$\mu_1 = \sqrt{1 - \frac{1 - \mu_0^2}{n_w^2}} \quad (16)$$

The reflectance factor RF and spherical albedo (SA) were calculated using both the numerical (IIM) (Mishchenko et al., 1999) and analytical (QSSA) methods. The QSSA method was applied in the form of eq 3 for RF and in the following form for SA (Sokoletsky and Kokhanovsky, 2005):

$$\text{SA}(\omega_0, F) = \frac{\omega_0}{1 - \omega_0 F} \sum_{i=0}^N \int_0^1 (-1)^i x_i P_i(\mu_1) Q_i(\mu_1) \mu_1 d\mu_1, \quad (17)$$

where x_i and $P_i(\theta)$ are the Fourier-Legendre coefficients and Legendre polynomials, respectively, for a given phase function $p(\theta)$ represented by the finite Fourier-Legendre series

$$p(\theta) = \sum_{i=0}^N x_i P_i(\theta), \quad (18)$$

corresponding with the normalization condition

$$\frac{1}{2} \int_0^\pi p(\theta) \sin \theta d\theta = 1. \quad (19)$$

The function $Q_i(\mu_1)$ was determined as (Sokoletsky and Kokhanovsky, 2005)

$$Q_i(\mu_1) = \int_0^1 \frac{P_i(\mu_2) \mu_2 d\mu_2}{\mu_1 + \mu_2}. \quad (20)$$

The following assumptions and parameters were incorporated into calculations: (a) plane parallel and flat water surface; (b) semi-infinite water layer; (c) strong nadir direction of water viewing ($\mu_2 = 1$); (d) negligible scattering by water molecules in relation to the total scattering; (e) the range of single-scattering albedo $\omega_0 \in [0.1; 0.99]$; and (f) the range of solar zenith angles $\theta_0 \in [0^\circ; 61.7^\circ]$. Two particulate scattering phase functions $p(\theta)$ with the backscattering ratio $B_p = b_{bp}/b_p = 0.0588$ (Kokhanovsky and Sokoletsky, 2006a) and $B_p = 0.0163$ (Haltrin, 1998b; Mobley et al., 2002; Sokoletsky et al., 2009) were used to represent typical Case 1 and Case 2 waters, respectively. The second $p(\theta)$ is the well established Fournier-Forand-Mobley (FFM) particulate scattering phase function. Selected parameters B_p and ω_0 yield Gordon's parameter $G = b_b/(b_b + a) = B_p \omega_0 / [1 - (1 - B_p) \omega_0]$ ranging from 0.002 to 0.617 to represent all possible natural situations including extremely turbid coastal waters (Haltrin and Gallegos, 2003).

Fig. 8 shows reflectance factor RF and spherical albedo SA computed as functions of G -parameter by the numerical (IIM) and analytical (QSSA) methods at FFM $p(\theta)$. Both the RF (Fig. 8a,b) and SA (Fig. 8c) are linearly proportional to G in the QSSA approximation. However, numerical calculations yield a sharper non-linear dependence for RF (Fig. 8a,b) than analytical calculations that can be explained by the increasing contribution of the multiple scattering. This increase, in turn, simultaneously increases backscattering, resulting in the increase of parameter G . But, at relatively small G values, the relationships are quite linear, independent of the approach. Another important feature of RF is its weak dependence on solar position (Fig. 8a,b).

From eqs 12 and 13 it follows that r_{rs} resembles the above-mentioned features of RF and SA. Indeed, numerical calculations revealed non-linear dependence of r_{rs} at increasing values of G and a small variation of r_{rs}

with θ_0 (Fig. 9). More specifically, variations in r_{rs} (expressed as the standard deviation relative to the mean) with θ_0 were within the range of 2.4–8.5% at a selected FFM phase function and at any values of ω_0 and λ from the above-mentioned ranges.

The spectral variability of r_{rs} resulting from the spectral variability of diffuse irradiance parameter d_E (eqs 12 and 13), was even smaller. For example, a variability of r_{rs} spectra, computed for the FFM $p(\theta)$ within the 560–709 nm spectral range, varied from 0.5% to 2.7% for any values of ω_0 and θ_0 across selected ranges. Thus, neglecting spectral impact, the following approximated expression for r_{rs} versus G was derived for the FFM $p(\theta)$:

$$r_{rs} = a_0 G(1 + a_1 G + a_2 \mu_1 + a_3 \mu_1^2) \quad (21)$$

where $a_0 = 0.2575$, $a_1 = 0.2757$, $a_2 = -0.7405$, $a_3 = 0.3610$ for Case 1 waters; $a_0 = 0.2874$, $a_1 = 0.2821$, $a_2 = -1.019$, $a_3 = 0.4561$ for Case 2 waters.

Compared with the numerical results, eq 21 yields $R^2 = 0.9994$ and a mean-normalized root-mean-squares error NRMSE = 1.7% for Case 1 waters, and $R^2 = 0.9998$, NRMSE = 2.1% for Case 2 waters.

Results obtained from eq 21 correspond well with the other approximations (Fig. 4, Table 1) for both water cases. Specifically, for more important Case 2 waters, the mean-normalized root-mean-squares difference (NRMSD) was <20% for r_{rs} derived from eq 21 and seven of the eleven other approximations listed in Table 1. Similarly, a comparison of results derived from all approximations listed in Table 1 with the numerically (IIM) calculated values of r_{rs} for FFM phase function yielded NRMSE <21% for 7 of 12 approximations. Another statistical measure—the coefficient of variation (CV = Standard Deviation/Mean) between all approximations—was 13%. This compared well with the literature value of 8.2% for 12 different Case 1 waters r_{rs} approximations (Sokoletsky, 2003). These findings indicate that a stable relationship exists between the Gordon's parameter G and r_{rs} for the wide variety of natural waters. Accordingly, Gordon's parameter is the principal factor regulating reflective properties in all natural waters (Haltrin and Gallegos, 2003).

Also, an eq 21 satisfies boundary condition: $\lim_{G \rightarrow 0} r_{rs}(G) = 0$ like most approximations (excluding only an approximation by Jerome et al. (1996), eq 4). However, at $G = 1$, eq 21, Case 2 waters yields $r_{rs} = 0.21$ –0.22 while the IIM gives $r_{rs} \approx 1/\pi \approx 0.32$. The better solutions at $G = 1$ yield approximations derived by Lee et al. (1999; $r_{rs} = 0.25$), Forget (2000; $r_{rs} = 0.29$), and Albert and Gege (2006; $r_{rs} = 0.26$ –0.27 depending on μ_1). The last three approximations were also among

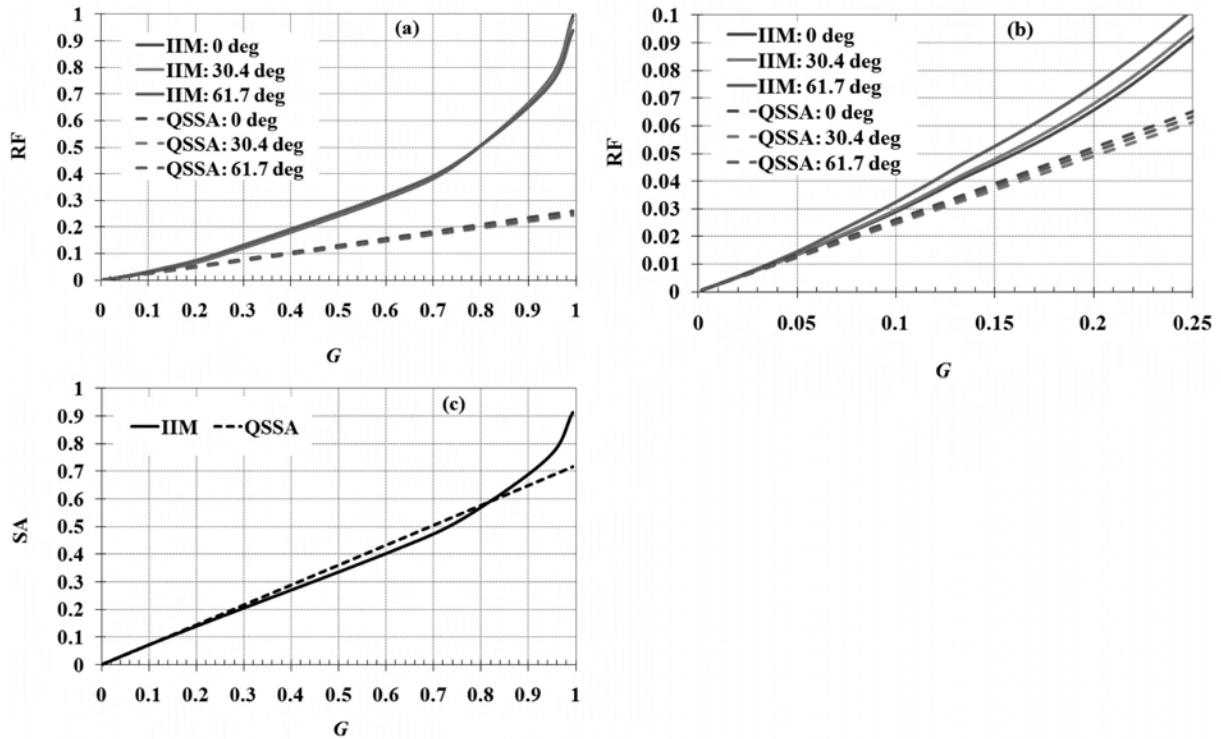


Fig. 8. Relationships between the Gordon's parameter G and: (a) reflectance factor RF for the entire range of G ; (b) reflectance factor RF for the range of G following from the NRE measurements; (c) spherical albedo SA. All calculations were carried out by the numerical (IIM) and analytical (QSSA) methods for the FFM scattering phase function, single-scattering albedo $\omega_0 \in [0.1; 0.99]$, solar zenith angles $\theta_0 = \{0^\circ, 30.4^\circ, 61.7^\circ\}$, and a nadir viewing angle θ_2 .

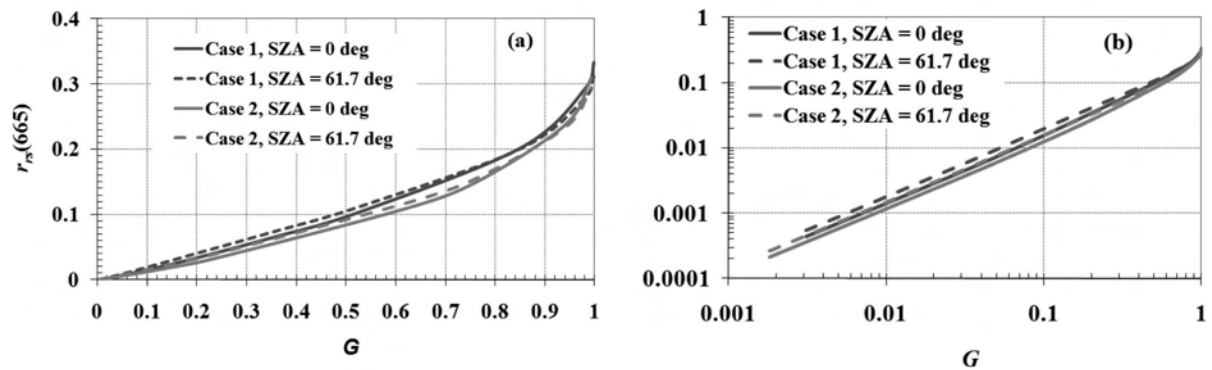


Fig. 9. Relationships between subsurface remote-sensing reflectance $r_{rs}(665)$ and Gordon's parameter G at selected solar zenith angles (SZA) θ_0 and two $p(\theta)$ simulating Case 1 and 2 waters. Calculations were made by IIM and presented in both linear (a) and logarithmic (b) scales.

closest to the numerical calculations and to our approximation (eq 21, Case 2 waters). Eq 21 for Case 2 waters yields ranges of G_{max} at which a deviation of r_{rs} versus G from linear dependency is still $<5\%$, $G_{max} \in [0.078; 0.087]$. This yields $r_{rs}(G_{max}) \in [0.0102; 0.0130]$ for $\theta_0 \in [0^\circ; 61.7^\circ]$.

Figure 10 illustrates the relationship between the r_{rs} ($\lambda = 665$ nm) and plane albedo PA. Calculations were performed using the IIM method (Kokhanovsky and Sokoletsky, 2006b; Sokoletsky et al., 2009) for the both $p(\theta)$ previously mentioned. The plot shows that r_{rs} may be well approximated by a simple expression, $r_{rs} =$

PA/π , independently of selected phase function and at any solar zenith angles. However, this equality holds more strongly when θ_0 is close to 60° .

Underwater optical algorithm development

An underwater semi-empirical optical algorithm was developed based on measured r_{rs} spectra. Only three wavelengths (560, 665, and 709 nm) corresponding to MERIS bands 5, 7, and 9 (Curran and Steele, 2005), were used for algorithm development. The following assumptions were applied in this study:

- a. The total absorption coefficient in the visible range (a_{vis}) is dominated by absorption of pure water, TSS (including Chl), and CDOM:

$$a_{vis} = a_{w,vis} + a_{TSS,vis} + a_{CDOM,vis}; \quad (22)$$

- b. The total absorption coefficient in the near infrared (NIR) spectral range (a_{NIR}) is dominated by absorption of pure water and CDOM:

$$a_{NIR} = a_{w,NIR} + a_{CDOM,NIR}; \quad (23)$$

- c. The backscattering coefficient is spectrally indepen-

dent over the limited red/NIR range:

$$b_{b,red} = b_{b,NIR} = b_b; \quad (24)$$

- d. The $a_{TSS,red}$ is the function of Chl, VSS, and TSS concentrations as follows:

$$a_{TSS,red} = a_4 \text{Chl} = a_5 \text{VSS}^{a_6} = a_7 \text{TSS}^{a_8} \quad (25)$$

The above assumptions are considered to be more rigorous than those previously used in the similar WQCs algorithms (Gons, 1999; Peters et al., 2002; Ruddick et al., 2001; Cauwer et al., 2004; Dall'Olmo and Gitelson, 2005). Specifically, a_{CDOM} was assumed to be zero in the red and NIR domains (Gons, 1999; Peters et al., 2002; Ruddick et al., 2001; Cauwer et al., 2004) or was assumed that $a_{CDOM,red} + a_{NAP,red} = a_{CDOM,NIR} + a_{NAP,NIR}$ (Dall'Olmo and Gitelson, 2005). By assuming that the absorption of CDOM and NAP decreases approximately exponentially with a wavelength (Lee et al., 1999; Dall'Olmo and Gitelson, 2005; Vähätalo et al., 2005; Astoreca et al., 2006), the last equality should be rewritten as inequality $a_{CDOM,NIR} + a_{NAP,NIR} < a_{CDOM,red} + a_{NAP,red}$.

Another simplification previously incorporated was

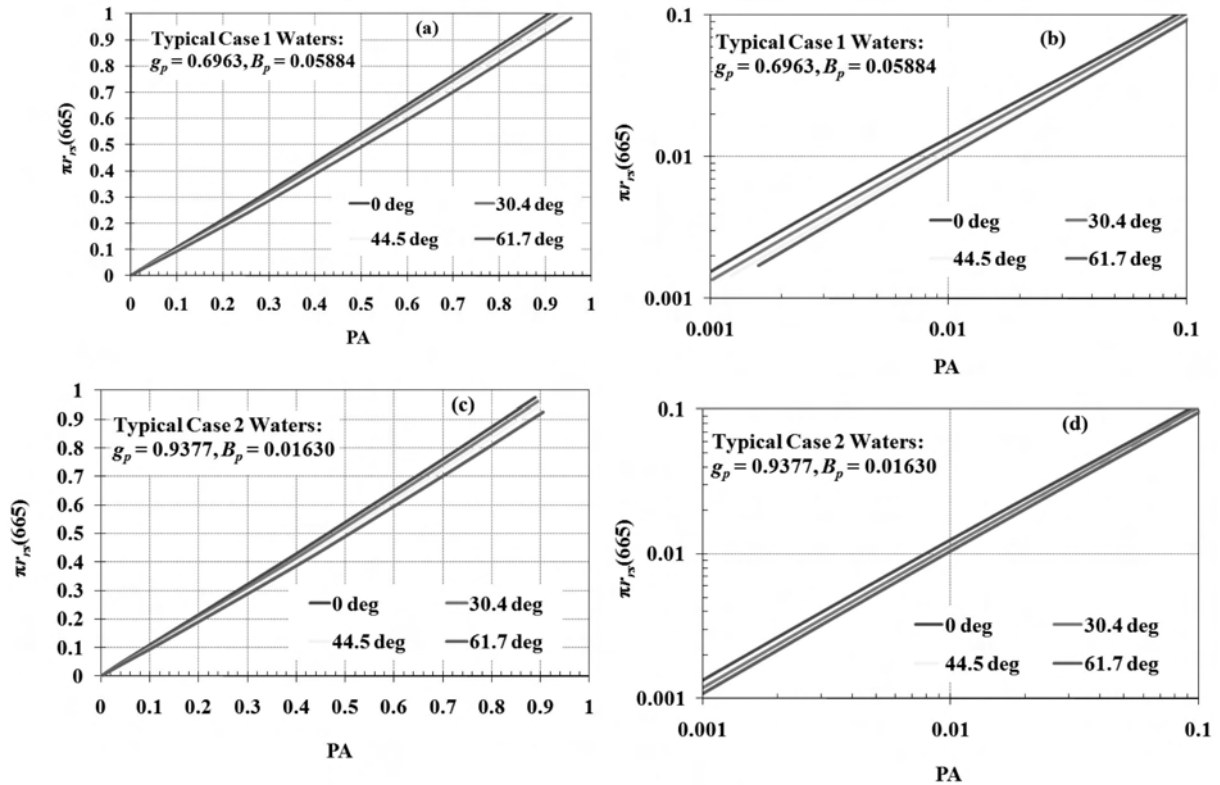


Fig. 10. Relationships between $\pi r_s(665)$ and PA at selected solar zenith angles θ_0 (on the legend) for the typical Case 1 (a, b) and Case 2 (c, d) waters in linear (a, c) and logarithmic (b, d) scales.

a direct proportionality between TSS concentration and its absorption coefficient (Gons, 1999; Peters et al., 2002; Ruddick et al., 2001; Cauwer et al., 2004; Dall'Olmo and Gitelson, 2005). However, our observations and modeling efforts yield non-linear power relationships between TSS and $a_{TSS,red}$ (Fig. 11a). Similarly, power dependence had been found between VSS and $a_{TSS,red}$ (Fig. 11b), although a relationship between Chl and $a_{TSS,red}$ can be best described by a linear dependence (Fig. 11c).

The final algorithm was constructed as follows:

$$\text{Chl} = a_{TSS}(665)/a_4, \quad \text{VSS} = [a_{TSS}(665)/a_5]^{1/a_6},$$

$$\text{TSS} = [a_{TSS}(665)/a_7]^{1/a_8}, \quad \text{FSS} = \text{TSS} - \text{VSS}, \quad (26)$$

$$a_{CDOM}(\lambda) = a_{CDOM}(412.5)(412.5/\lambda)^{1/a_9}, \quad (27)$$

where

$$a_{CDOM}(412.5) = a_{10} [G(665) / G(665)]^{1/a_{11}}, \quad (28)$$

$$a_{TSS}(665) = \left[\frac{1/G(665) - 1}{1/G(709) - 1} \right] [a_w(709) + a_{CDOM}(709)] - [a_w(665) + a_{CDOM}(665)], \quad (29)$$

$$G(\lambda) = 0.5 \left[\sqrt{F_1^2 + F_2(\lambda)} - F_1 \right] / a_1, \quad F_1 = 1 + a_2\mu_1 + a_3\mu_1^2,$$

$$F_2(\lambda) = 4a_1r_{rs}(\lambda) / a_0 \quad (30)$$

The underwater optical algorithm expressed by eqs 26–30 did not include a calculation of the backscattering coefficient b_b . However, the b_b may be calculated separately:

$$b_b = \frac{[a_w(709) + a_{CDOM}(709)] G(709)}{1 - G(709)}, \quad (31)$$

Spectral values of pure water absorption were derived by linear interpolation among values obtained by Kou et al. (1993) and by Pope and Fry (1997). A simple power model for CDOM absorption spectra (eq 27) was derived to provide more precise results than the traditional exponential model. A similar conclusion was reached by Twardowski et al. (2004) based on measurements from around the coastal United States. For comparison, analysis of all 135 samples collected at the NRE stations yields $a_9 = 7.13 \pm 0.78$, that is very similar to the results reported by Twardowski et al. (2004) ($a_9 = 6.92 \pm 0.39$).

The parameterization of the underwater optical algorithm (eqs 26–31) was realized through the comparison of modeling [at Case 2 waters FFM $p(\theta)$] and observed WQCs values using the least-squares method (Table 2).

The Gordon's parameter G was a key algorithmic parameter. Equation 30 relates measured spectral remote-sensing reflectance r_{rs} (apparent optical property) to the cosine (μ_1) of the solar zenith angle just under water and Gordon's parameter G (inherent optical property). Therefore, the parameter G can be calculated by inversion of r_{rs} , using easily accessible value of μ_1 . Having G in hand, WQCs are directly computed by using eqs 26–29.

Underwater optical algorithm validation

The underwater optical algorithm was validated by visual comparison of Chl collected from ModMon station #120 with values derived from our model for the same location (Fig. 3c). The plot demonstrates the close correspondence of Chl values for these two datasets and suggests a high predictive power for the model. Two additional validation methods included estimating (i) potential errors associated with the estimation, and (ii) WQCs errors values yielding by comparison the algorithm's estimates with the ModMon results. We assessed the impact of three different error sources on $a_{TSS,red}$ retrieval accuracies. The assumptions of $a_{CDOM,red} = a_{CDOM,NIR} = 0$ and $G_{NIR}/G_{red} = r_{rs,NIR}/r_{rs,red}$ were made (Gons, 1999; Peters et al., 2002; Ruddick et al., 2001; Cauwer et al., 2004), while the third source of errors was the definite particulate scattering phase function (FFM). The first assumption yields the relative error, which can be expressed from eq 29 as follows:

$$\delta a_{TSS,red} = \frac{a_{CDOM,red} - F a_{CDOM,NIR}}{a_{TSS,red}} 100\%,$$

$$F = \left[\frac{1/G(665) - 1}{1/G(709) - 1} \right]. \quad (32)$$

Numerical results indicated that $\delta a_{TSS,red} \geq 50\%$ at small values of $a_{TSS,red}$. However, errors quickly declined to 10% at $a_{TSS,red} > 0.5 \text{ m}^{-1}$ (Fig. 12). These findings correspond to those found by Astoreca et al. (2006). To estimate the accuracy of the QSSA approximation for $a_{TSS}(665)$, we rewrote eq 29 in the form:

$$a_{TSS}(665) = \frac{r_{rs}(709)}{r_{rs}(665)} [a_w(709) + a_{CDOM}(709) + b_b] - [a_w(665) + a_{CDOM}(665) + b_b] \quad (29')$$

Our analysis indicated relatively small errors for $\delta a_{TSS}(665)$ retrieval by eq 29' (Fig. 12). The overall range of errors was between -7.5% and 11.0% with the NRMSE of 13.9%.

Calculated r_{rs} for Case 2 waters $p(\theta)$ were compared with r_{rs} Case 1 waters $p(\theta)$ to assess the relative errors that were attributable to the FFM $p(\theta)$. Figure 9 shows that individual values of r_{rs} calculated at the same G vary

Table 2
Parameters of the underwater optical algorithm used for the study

Model Parameter	Value	Units
a_0	0.2874	sr ⁻¹
a_1	0.2821	—
a_2	-1.019	—
a_3	0.4561	—
a_4	0.01649	m ² mg ⁻¹
a_5	0.08712	m ² g ⁻¹
a_6	1.153	—
a_7	0.005580	m ² g ⁻¹
a_8	1.984	—
a_9	-7.063	—
a_{10}	4.791	m ⁻¹
a_{11}	1.218	—
$a_w(665)$	0.429	m ⁻¹

significantly with $p(\theta)$. Relative errors were in the range of -23% to -2.7% and NRMSE = 16% at $\lambda = 665$ nm, $G \in [0.001; 1]$ and $\theta_0 \in [0^\circ; 61.7^\circ]$. Nevertheless, logarithmic curves of r_{rs} built for two different $p(\theta)$, but with the same θ_0 were almost parallel (i.e., displaced by an almost constant offset), approximately up to $G = 0.7$ (Fig. 9b). Thus, the spectral G -ratios will be only weakly depend on selected $p(\theta)$ (Sokoletsky and Gallegos, 2010). Consequently, relative errors (δ) in computed $a_{TSS}(665)$ for the Case 2 waters $p(\theta)$ were comparable to those computed for the Case 1 waters $p(\theta)$ at $\delta \in [-0.7\%; 1.2\%]$ (Fig. 12). Thus, the impact of $p(\theta)$ on the retrieval WQCs was absolutely insignificant for our data.

A comparison of WQCs predicted by the underwater optical algorithm with observed (ModMon) WQCs values for different NRE collection dates indicated relatively good results for a_{CDOM} , Chl, VSS and TSS, and poor results for FSS (Fig. 13). To obtain a quantitative

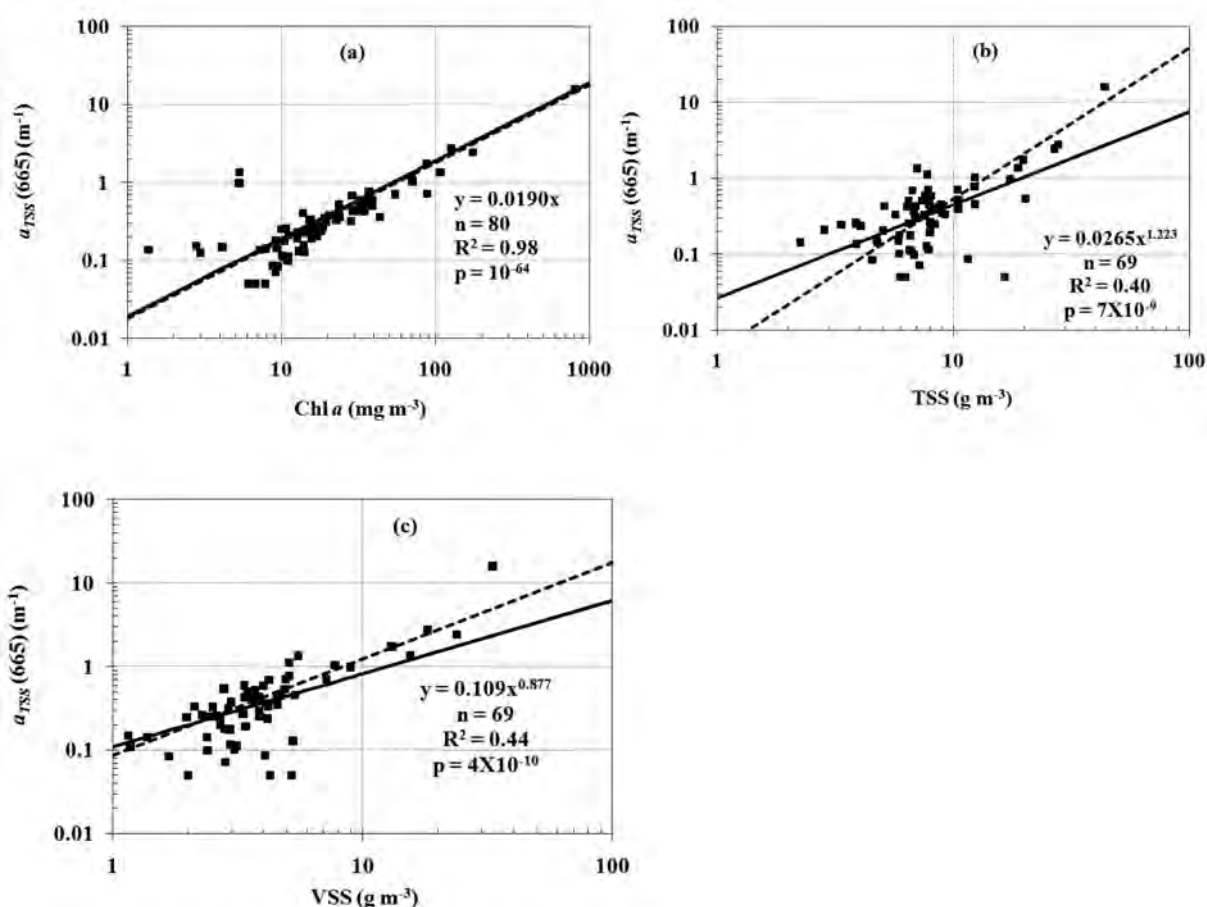


Fig. 11. Relationships between $a_{TSS}(665 \text{ nm})$ and Chl (a), TSS (b), and VSS (c) in NRE between October 2006 and October 2008 (symbols and solid curves). The relationships pertaining to the underwater optical model are shown by the dashed curves.

estimate, several statistical characteristics were applied, including the mean, standard deviation (SD), coefficient of variation (CV), mean biased error (MBE), mean biased error normalized to the mean measured value (NMBE), RMSE, NRMSE, R^2 , significance level p , and intercept and slope of the regression line (Table 3).

The MBE and RMSE were calculated using

$$MBE = \frac{\sum_{i=1}^n (x_i - \bar{x}_i)}{n-1}, \quad (33)$$

$$RMSE = \sqrt{\frac{\sum_{i=1}^n (x_i - \bar{x}_i)^2}{n-1}}, \quad (34)$$

where x_i and \bar{x}_i are observed and predicted WQC for the i^{th} sample, respectively; n is the sample size for given WQC. Other characteristics were calculated using standard Microsoft Excel functions. For example, for calculation of p , a standard function TDIST(t , DF, T) has been used, where its parameters are defined as follows (Spiegel and Stephens, 2008): t is the parameter of the Student t -distribution

$$t = R \sqrt{\frac{DF}{1-R^2}}, \quad (35)$$

DF = $n - 2$ is degree of freedom, and T is the number of distribution tails ($T = 2$ accepted).

The statistical analysis indicated that all WQCs were quite variable, with a maximum of CV for Chl of 105% and minimum for $a_{CDOM}(412.5)$ of 54% (Table 3). The

lowest (35%) and highest (59%) NRMSE errors were obtained for $a_{CDOM}(412.5)$ and FSS, respectively. However, minimal NMBE was determined for FSS (1.3%) and maximum for VSS (-6.6%). The best values of R^2 , p and slope were found for Chl, while the worst for FSS.

DISCUSSION AND CONCLUSIONS

An analytical equation for remote-sensing reflectance r_{rs} that incorporates both RF and SA has been derived (eq 12). This equation, together with numerical calculations carried out using an invariant imbedding method to solve the radiative transfer equation, has resulted in a new equation relating r_{rs} with the Gordon's parameter G and cosine μ_1 of the solar zenith angle θ_1 after refraction on the air-water surface (eq 21). An analysis of this equation for Case 2 waters indicated that it may be considered linear (with 5% accuracy) for $G < 0.078-0.087$ that corresponds to $r_{rs} < 1.1\%$. As a result, simple linear models for r_{rs} , as a sole function of G , can be accurately applied to analyze a variety of water bodies. Furthermore, using the spectral r_{rs} or G ratios instead of individual spectral values significantly reduces errors related to r_{rs} (G) nonlinearity.

Similar conclusions can be drawn concerning the particulate scattering phase function $p(\theta)$ impact on the calculated r_{rs} . Although the differences between r_{rs} computed at different $p(\theta)$ may be relatively large (Fig. 9a), spectral G ratios would be only weakly influenced by $p(\theta)$ (Fig. 9b). Therefore, the calculation of $a_{TSS}(665)$ and WQCs would also be weakly influenced by $p(\theta)$ (Fig. 12). These findings were also confirmed by the radiative transfer computations carried out by Lee et

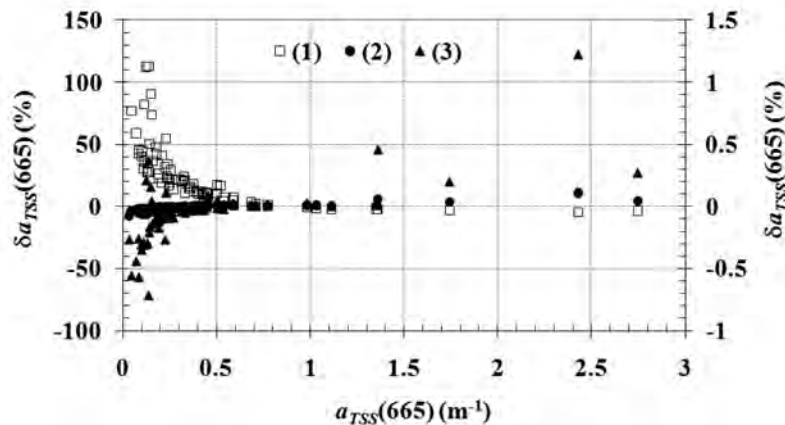


Fig. 12. Relative errors of TSS absorption $a_{TSS}(665)$ as a function of $a_{TSS}(665)$ for the NRE under using three different assumptions: (1) $a_{CDOM,red} = a_{CDOM,NIR} = 0$, (2) $G(709)/G(665) = r_{rs}(709)/r_{rs}(665)$ and (3) FFM $p(\theta)$. Assumptions are presented on the left (1 and 2) and right (3) ordinate axes.

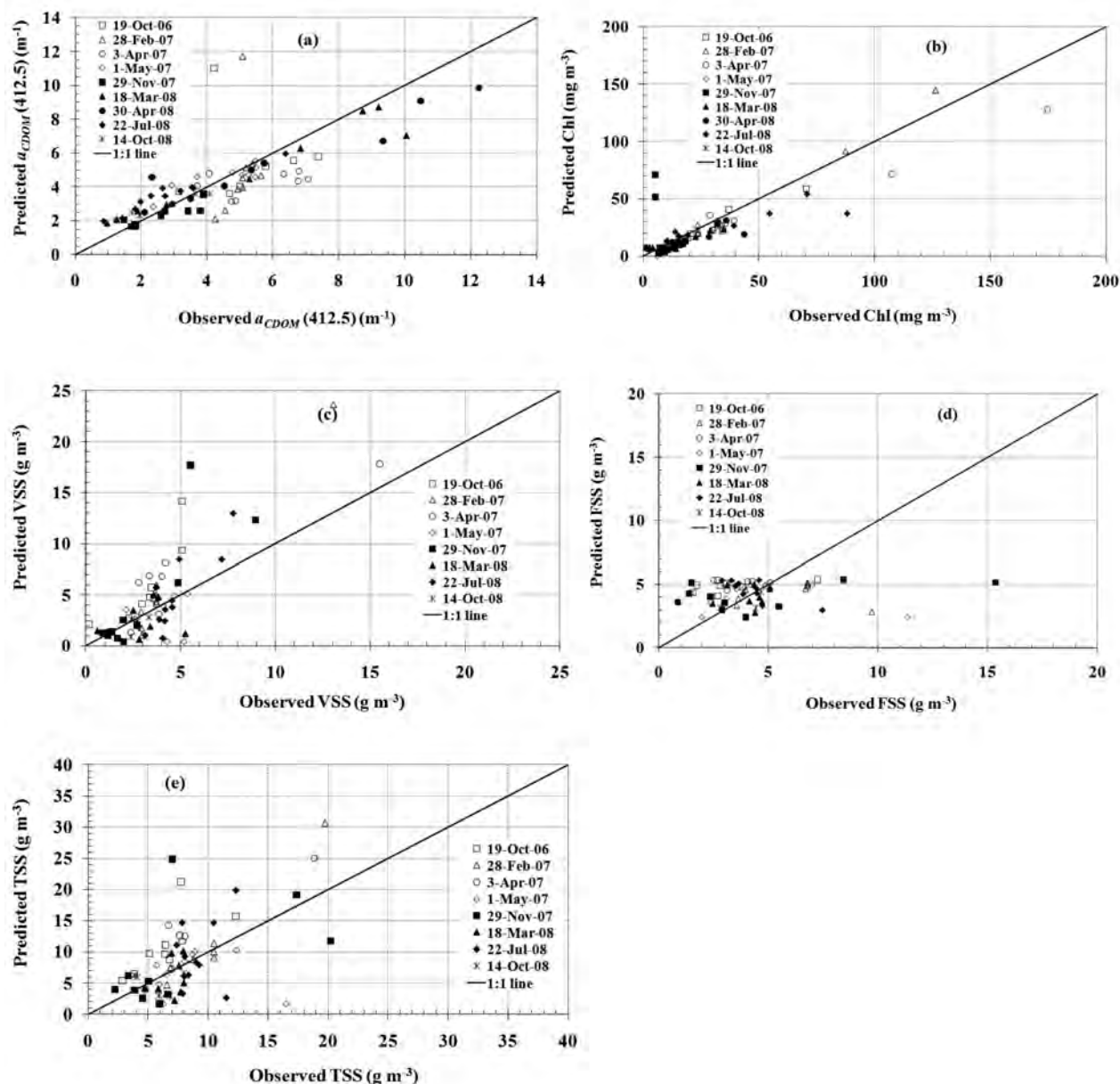


Fig. 13. Comparison of predicted versus observed (ModMon) WQCs values in the NRE for CDOM absorption (a), Chl (b), VSS (c), FSS (d), and TSS (e).

al. (1998). However, the impact of an incorrect model for CDOM absorption may be very large (Fig. 12). This important issue needs to be taken into account in the development of new optical models for turbid waters.

The results of this study indicate that r_{rs} may be accurately represented in the form of PA/π . This relationship holds strongly for solar zenith angles θ_0 close to 60° independently on selected $p(\theta)$ (Fig. 10). This conclusion may be useful for further hydrologic optics work.

An analysis of the optical and water quality measurements in the APES, along with a consideration of the radiative transfer within the water column and at the air-water interface, led to the development of a semi-empirical water quality algorithm for this region (eqs 26–30). The algorithm utilizes three wavelengths (560, 665, and 709 nm) that correspond to the MERIS bands 5, 7, and 9. The algorithm validation yielded acceptable results for WQCs that included Chl, VSS, TSS concen-

Table 3

Statistical characteristics of measured and predicted WQCs used to support the in-water optical model for the Neuse River Estuary. *n*, Mean, SD and CV are the sample size, measured mean, standard deviation, and coefficient of variation, respectively. The mean biased error MBE (eq 33) and the root-mean-squares error RMSE (eq 34) show absolute errors of predicted values relative to measured ones. The NMBE and NRMSE show corresponding normalized (to the measured mean) errors. Determination coefficient R^2 , significance level p , intercept and slope demonstrate degree of correlation between predicted and measured WQCs

WQC	<i>n</i>	Mean (mg m ⁻³)	SD (mg m ⁻³)	CV (%)	NMBE (%)	NRMSE (%)	R^2	p	Intercept (mg m ⁻³)	Slope
$a_{\text{CDOM}}(412.5)$ (m ⁻¹)	79	4.4	2.3	54	-3.2	35	0.59	2×10^{-16}	1.3	0.68
Chl (mg m ⁻³)	79	27.7	29.1	105	-5.2	36	0.88	7×10^{-38}	0.60	0.93
VSS (g m ⁻³)	68	4.4	3.8	87	-6.6	42	0.78	3×10^{-23}	0.36	0.85
FSS (g m ⁻³)	68	4.3	2.4	56	1.3	59	0.00	0.89	4.3	0.01
TSS (g m ⁻³)	68	8.6	4.9	57	-2.7	40	0.51	6×10^{-12}	3.4	0.58

trations and CDOM absorption. However, our attempt to derive FSS concentration was not successful (Table 3). Relatively large errors obtained for the WQCs maybe directly attributable to the natural variability of optical properties of particulate and dissolved matter (Fig. 11). Also, in-situ radiometric and WQCs measurements errors may have been a contributing factor (Toole, 2000; Ouillon and Petrenko, 2005).

The choice between completely empirical and semi-empirical algorithms to support current and future monitoring needs represents an important issue. Although it is well known that empirical algorithms often lead to equal or even better results than semi-empirical algorithms, we chose a semi-empirical algorithm because it generally provides better spatial and temporal robustness. Furthermore, we believe that is possible to enhance our semi-empirical algorithm by parameterizing the algorithm to account for specific water features and properties for application at other locations. We expect that the underwater optical algorithms similar to the one derived in the current investigation will work better for the water bodies with some correlations between constituents. The findings obtained in this study are important for the development of a remote-sensing algorithm for monitoring WQCs in the APES (Sokoletsky et al., 2011) and other inland and coastal waters.

ACKNOWLEDGMENTS

This article is devoted to the 70th birthday of Prof. Anatoly Gitelson, who was the patient and wise supervisor as well as remote sensing mentor for one of the authors (LGS). We also would like to acknowledge him, and Peter Principe and Megan VanFossen as well, for their manuscript review comments and suggestions. We thank Alexander Kokhanovsky for making available the

results of his radiative transfer calculations. Also, thanks are extended to Joseph Knight, Benjamin Peierls, Pam Wyrick, and Jeremy Braddy for providing ModMon water quality data; and to Rodney Guajardo for providing FerryMon chlorophyll *a* data. The United States Environmental Protection Agency (USEPA) funded and partially conducted the research described in this paper. The USEPA provided funding to the National Research Council in support of this effort under Cooperative Agreement #CR-833232. Partial research funding was provided by the USEPA Global Earth Observation System of Systems (GEOSS) Advanced Monitoring Initiative (AMI) Grant #14. Although this work was reviewed by EPA and has been approved for publication, it may not necessarily reflect official Agency policy. Mention of any trade names or commercial products does not constitute endorsement or recommendation for use.

REFERENCES

- Aas, E. 1987. Two stream irradiance model for deep waters. *Appl. Opt.* 26: 2096–2101.
- Aas, E., Højerslev, N.K. 1999. Analysis of underwater radiance observations: Apparent optical properties and analytic functions describing the angular radiance distribution. *J. Geophys. Res.* 104: 8015–8024.
- Albert, A., Gege, P. 2006. Inversion of irradiance and remote sensing reflectance in shallow water between 400 and 800 nm for calculations of water and bottom properties. *Appl. Opt.* 45: 2331–2343.
- Anikonov, A.S., Ermolaev, S.Y. 1977. On diffuse light reflection from a semiinfinite atmosphere with a highly extended phase function. *Vestnik LGU* 7: 131–137.
- Astoreca, R., Ruddick, K., Rousseau, V., Van Mol, B., Parent, J.-Y., Lancelot, C. 2006. Variability of the inherent and apparent optical properties in a highly turbid coastal area: impact on the calibration of remote sensing algorithms. *EARSeL eProceedings* 5: 1–17.

- Babin, M., Stramski, D. 2002. Light absorption by aquatic particles in the near-infrared spectral region. *Limnol. Oceanogr.* 47: 911–915.
- Borsuk, M.E., Stow, C.A., Reckhow, K.H. 2003. Integrated approach to Total Maximum Daily Load development for Neuse River Estuary using Bayesian Probability Network Model (Neu-BERN). *ASCE Journal of Water Resources Planning and Management* 131: 271–282.
- Burkholder, J., Eggleston, D., Glasgow, H., Brownie, C., Reed, R., Janowitz, G., Posey, M., Melia, G., Kinder, C., Corbett, R., Toms, D., Alphin, T., Deamer, N., Springer, J. 2004. Comparative impacts of two major hurricane seasons on the Neuse River and western Pamlico Sound ecosystems. *Proc. Natl. Acad. Sci. USA* 101: 9291–9296.
- Boynton, G.C., Gordon, H.R. 2000. Irradiance inversion algorithm for estimating the absorption and backscattering coefficients of natural waters: Raman-scattering effects. *Appl. Opt.* 39: 3012–3022.
- Buzzelli, C.P., Ramus, J.R., Paerl, H.W. 2003. Ferry-based monitoring of surface water quality in North Carolina estuaries. *Estuaries* 26: 975–984.
- Cauwer, V.D., Ruddick, K., Park, Y.J., Kyramarios, M. 2004. Optical remote sensing in support of eutrophication monitoring in the Southern North Sea. *EARSel eProceedings* 3: 208–221.
- Copeland, B.J., Gray, J. 1991. Status and trends of the Albemarle-Pamlico Estuary study. Tech. Report Number 90–01. Department of Environment, Health, and Natural Resources, Raleigh, NC State University, NC, USA.
- Craig, S.E., Lohrenz, S.E., Lee, Z.P., Mahoney, K.L., Kirkpatrick, G.J., Schofield, O.M., Steward, R.G., 2006. Use of hyperspectral remote sensing reflectance for detection and assessment of the harmful alga, *Karenia brevis*. *Appl. Opt.* 45: 5414–5425.
- Curran, P.J., Steele, C.M. 2005. MERIS: the re-branding of an ocean sensor. *Int. J. Remote Sens* 26: 1781–1798.
- Dall’Olmo, G., Gitelson, A.A., 2005. Effect of bio-optical parameter variability on the remote estimation of chlorophyll-*a* concentration in turbid productive waters: experimental results. *Appl. Opt.* 44: 412–422.
- Duffie, J.A., Beckman, W.A. 2006. *Solar engineering of thermal processes*, 3rd ed. Wiley & Sons, New York.
- Eaton, A.D., Clesceri, L.S., Rice, E.W., Greenberg, A.E., eds., 2005. *Standard methods for the examination of water and wastewater*, 21st ed. American Public Health Association, American Water Works Association and Water Environment Federation, Washington, DC.
- Exell, R.H.B. 1981. A mathematical model for solar radiation in South-East Asia (Thailand). *Solar Energy* 26: 161–168.
- Forget, P. 2000. An analytical model of remote sensing reflectance in coastal zone and application to water constituents retrieval with MERIS. In: *Proceedings of Ocean Optics XV Conference*, 16–20 October 2000, Monaco (CD-ROM, No. OO1039).
- Gallegos, C.L., Jordan, T.E., Hines, A.H., Weller, D.E., 2005. Temporal variability of optical properties in a shallow, eutrophic estuary: seasonal and interannual variability. *Estuar. Coast. Shelf S.* 64: 156–170.
- Gitelson, A.A., Schalles, J.F., Hladik, C.M. 2007. Remote chlorophyll-*a* retrieval in turbid, productive estuaries: Chesapeake Bay case study. *Remote Sens. Environ.* 109: 464–472.
- Gons, H.J. 1999. Optical teledetection of chlorophyll *a* in turbid inland waters. *Environ. Sci. Technol.* 33: 1127–1133.
- Gordon, H.R. 1973. Simple calculation of the diffuse reflectance of ocean. *Appl. Opt.* 12: 2803–2804.
- Gordon, H.R. 1976. Radiative transfer in the ocean: a method for determination of absorption and scattering properties. *Appl. Opt.* 15: 2611–2613.
- Gordon, H.R. 1992. Diffuse reflectance of the ocean: influence of nonuniform phytoplankton pigment profile. *Appl. Opt.* 31: 2116–2129.
- Gordon, H.R., Brown, O.B. 1974. Influence of bottom depth and albedo on the diffuse reflectance of a flat homogeneous ocean. *Appl. Opt.* 13: 2153–2159.
- Gordon, H.R., Brown, O.B. 1975. Diffuse reflectance of the ocean: some effects of vertical structure. *Appl. Opt.* 14: 2892–2895.
- Gordon, H.R., Brown, O.B., Jacobs, M.M. 1975. Computed relationships between the inherent and apparent optical properties of a flat homogeneous ocean. *Appl. Opt.* 14: 417–427.
- Gordon, H.R., Brown, O.B., Evans, R.H., Brown, J.W., Smith, R.C., Baker, K.S., Clark, D.K. 1988. A semi-analytical radiance model of ocean color. *J. Geophys. Res.* 93: 10909–10924.
- Jerome, J.H., Bukata, R.P., Miller, J.R. 1996. Remote sensing reflectance and its relationship to optical properties of natural waters. *Int. J. Remote Sens.* 17: 3135–3155.
- Haltrin, V.I. 1998a. Self-consistent approach to the solution of light transfer problem for irradiances in marine waters with arbitrary turbidity, depth, and surface illumination. I. Case of absorption and elastic scattering. *Appl. Opt.* 37: 3773–3784.
- Haltrin, V.I. 1998b. An analytical Fournier–Forand scattering phase function as an alternative to the Henyey–Greenstein phase function in hydrologic optics. In: Stein, T.I., ed., *Proceedings of the IEEE International Geoscience and Remote Sensing Symposium*, 11, July 6–10 1998, Seattle, WA, USA (Piscataway: IEEE), pp. 910–913.
- Haltrin, V.I., Gallegos, S.C. 2003. About nonlinear dependence of remote sensing and diffuse reflectance coefficients of Gordon’s parameter. In: Levin, I., Gilbert, G., eds., *Proceedings of D. S. Rozhdestvensky Optical Society Current Problems in Optics of Natural Waters, II International Conference*, 8–12 September 2003, St. Petersburg, Russia (St. Petersburg: State Optical Institute), pp. 363–369.
- Hapke, B. 1993. *Theory of reflectance and emittance spectroscopy*. Cambridge University Press, New York.
- Helyar, A.G. 2001. Equation of time, <http://homepages.pavilion.co.uk/aghelyar/sundat.htm>.
- Højerslev, N.K. 2001. Analytic remote-sensing optical algorithms requiring simple and practical field parameter inputs. *Appl. Opt.* 40: 4870–4874.
- Højerslev, N.K. 2004. Practical sea-water algorithms for fun-

- damental bio-optical and remote sensing quantities. *Int. J. Remote Sens.* 25: 1539–1543.
- Kirk, J.T.O. 1981. Monte Carlo study of the nature of the underwater light field in, and the relationships between optical properties of, turbid yellow waters. *Aust. J. Mar. Freshwater Res.* 32: 517–532.
- Kirk, J.T.O. 1991. Volume scattering function, average cosines, and the underwater light field. *Limnol. Oceanogr.* 36: 455–467.
- Kirk, J.T.O. 1994. Light and photosynthesis in aquatic ecosystems, 2nd ed. Cambridge University Press, NY.
- Kokhanovsky, A.A., Sokoletsky, L.G. 2006a. Reflection of light from semi-infinite absorbing turbid media. Part 1: Spherical albedo. *Color Res. Appl.* 31: 491–497.
- Kokhanovsky, A.A., Sokoletsky, L.G. 2006b. Reflection of light from semi-infinite absorbing turbid media. Part 2: Plane albedo and reflection function. *Color Res. Appl.* 31: 498–509.
- Kou, L., Labrie, D., Chylek, P. 1993. Refractive indices of water and ice in the 0.65 μm to 2.5 μm spectral range. *Appl. Opt.* 32: 3531–3540.
- Lee, Z.P., Carder, K.L., Mobley, C.D., Steward, R.G., Patch, J.S. 1998. Hyperspectral remote sensing for shallow waters. 1. A semianalytical model. *Appl. Opt.* 37: 6329–6338.
- Lee, Z.P., Carder, K.L., Mobley, C.D., Steward, R.G., Patch, J.S. 1999. Hyperspectral remote sensing for shallow waters. 2. Deriving bottom depths and water properties by optimization. *Appl. Opt.* 38: 3831–3843.
- Lee, Z.P., Carder, K.L., Du, K.P. 2004. Effects of molecular and particle scatterings on the model parameter for remote-sensing reflectance. *Appl. Opt.* 43: 4957–4964.
- Levin, I.M. 1998. Sea radiance coefficient: estimate of the quasi-single approximation. *Oceanology of the Russian Academy of Sciences* 38: 855–858.
- Mishchenko, M.I., Dlugach, J.M., Yanovitskij, E.G., Zakharova, N.T. 1999. Bidirectional reflectance of flat, optically thick particulate layers: an efficient radiative transfer solution and applications to snow and soil surfaces. *J. Quant. Spectrosc. Ra.* 63: 409–432.
- Mobley, C.D. 1999. Estimation of the remote-sensing reflectance from above-surface measurements. *Appl. Opt.* 38: 7442–7455.
- Mobley, C.D., Sundman, L.K., Boss, E. 2002. Phase function effects on oceanic light fields. *Appl. Opt.* 41: 1035–1050.
- Mobley, C.D., Stramski, D., Boss, E. 2004. Optical modeling of ocean water: is the Case 1—Case 2 classification still useful? *Oceanography* 17: 60–67.
- Morel, A. 1988. Optical modeling of the upper ocean in relation to its biogenous matter content (case 1 water). *J. Geophys. Res.* 93: 10,749–10,768.
- Morel, A., Gentili, B. 1991. Diffuse reflectance of oceanic waters: its dependence on Sun angle as influenced by the molecular scattering contribution. *Appl. Opt.* 30: 4427–4438.
- Morel, A., Gentili, B. 1993. Diffuse reflectance of oceanic waters. 2. Bidirectional aspects. *Appl. Opt.* 32: 6864–6879.
- Morel, A., Gentili, B. 1996. Diffuse reflectance of oceanic waters. 3. Implication of bidirectionality for the remote-sensing problem. *Appl. Opt.* 35: 4850–4862.
- Morel, A., Prieur, L. 1977. Analysis of variations in ocean color. *Limnol. Oceanogr.* 22: 709–722.
- Morel, A., Maritorena, S. 2001. Bio-optical properties of oceanic waters: a reappraisal. *J. Geophys. Res.* 106: 7163–7180.
- Morel, A., Antoine, D., Gentili, B. 2002. Bidirectional reflectance of oceanic waters: accounting for Raman emission and varying particle scattering phase function. *Appl. Opt.* 41: 6289–6306.
- Nicodemus, F. 1965. Directional reflectance and emissivity of an opaque surface. *Appl. Opt.* 4: 767–775.
- Otremba, Z. 2003. Relationships between the quantities which describe reflective features of both land and ocean areas. In: Levin, I., Gilbert, G., eds., *Proceedings of D.S. Rozhdestvensky Optical Society Current Problems in Optics of Natural Waters II International Conference*, 8–12 September, 2003, St. Petersburg, Russia (St. Petersburg: State Optical Institute), pp. 376–381.
- Ouillon, S., Petrenko, A.A. 2005. Above-water measurements of reflectance and chlorophyll-*a* algorithms in the Gulf of Lions, NW Mediterranean Sea. *Opt. Express* 13: 2531–2548.
- Paerl, H.W., Pinckney, J.L., Fear, J.M., Peierls, B.L. 1998. Ecosystem responses to internal and watershed organic matter loading: consequences for hypoxia in the eutrophying Neuse River Estuary, North Carolina, USA. *Mar. Ecol.: Prog. Ser.* 166: 17–25.
- Paerl, H.W., Bales, J.D., Ausley, L.W., Buzzelli, C.P., Crowder, L.B., Eby, L.A., Fear, J.M., Go, M., Peierls, B.L., Richardson, T.L., Ramus, J.S. 2001. Ecosystem impacts of three sequential hurricanes (Dennis, Floyd, and Irene) on the United States' largest lagoonal estuary, Pamlico Sound, NC. *Proc. Natl. Acad. Sci. USA* 98: 5655–5660.
- Paerl, H.W., Valdes, L.M., Piehler, M.F., Stow, C.A. 2006. Assessing the effects of nutrient management in an estuary experiencing climatic change: the Neuse River Estuary, NC, USA. *Environ. Manage.* 37: 422–436.
- Peters, S.W.M., Pasterkamp, R., van de Woerd, H.J. 2002. A sensitivity analysis of analytical inversion methods to derive chlorophyll from MERIS spectra in case-II waters. In *Proceedings of the Ocean Optics XVI Conference*, 18–22 November 2002, Santa Fe, NM, USA (Arlington: Office of Naval Research), pp. 363–369.
- Pope, R.M., Fry, E.S. 1997. Absorption spectrum (380–700 nm) of pure water. II. Integrating cavity measurements. *Appl. Opt.* 36: 8710–8723.
- Ruddick, K.G., Gons, H.J., Rijkeboer, M., Tilstone, G. 2001. Optical remote sensing of chlorophyll *a* in Case 2 waters by use of an adaptive two-band algorithm with optimal error properties. *Appl. Opt.* 40: 3575–3585.
- Quan, X., Fry, E.S. 1995. Empirical equation for the index of refraction of seawater. *Appl. Opt.* 34: 3477–3480.
- Smyth, T. J., Moore, G. F., Hirata, T, Aiken, J. 2006. Semi-analytical model for the derivation of ocean color inherent properties: description, implementation, and performance assessment. *Appl. Opt.* 45: 8116–8131.
- Sokoletsky, L. 2003. In situ and remote sensing bio-optical methods for the estimation of phytoplankton concentra-

- tion in the Gulf of Aqaba (Eilat). Ph.D. Thesis, Bar-Ilan University, Israel.
- Sokoletsky, L. 2004. A comparative analysis of simple transfer approaches for aquatic environments. In: Proceedings of the 2004 ENVISAT and ERS Symposium, 6–10 September 2004, Salzburg, Austria. CD-ROM.
- Sokoletsky, L. 2005. Comparative analysis of selected radiative transfer approaches for aquatic environments. *Appl. Opt.* 44: 136–148.
- Sokoletsky, L., Gallegos, S. 2010. Towards development of an improved technique for remote retrieval of water quality components: an approach based on the Gordon's parameter spectral ratio. In: Proceedings of Ocean Optics—XX Conference, 27 September–1 October 2010, Anchorage, Alaska, USA. CD-ROM.
- Sokoletsky, L.G., Kokhanovsky, A.A. 2005. Reflective characteristics of natural waters: the accuracy of selected approximations. In: Levin, I., Gilbert, G., eds., Proceedings of Current Problems in Optics of Natural Waters III International Conference, 12–16 September 2005, St. Petersburg, Russia, pp. 56–63.
- Sokoletsky, L.G., Nikolaeva, O.V., Budak, V.P., Bass, L.P., Lunetta, R.S., Kuznetsov, V.S., Kokhanovsky, A.A. 2009. Comparison of different numerical and analytical solutions of the radiative-transfer equation for plane albedo with emphasis on the natural waters consideration. *J. Quant. Spectrosc. Ra.* 110: 1132–1146.
- Sokoletsky, L.G., Lunetta, R.S., Wetz, M.S., Paerl, H.W. 2011. MERIS retrieval of water quality components in the turbid Albemarle–Pamlico Sound Estuary, USA. *Remote Sens.* 3: 684–707.
- Spiegel, M.R., Stephens, L.J. 2008. Theory and problems of statistics, 4th ed. Schaum's Outline Series, McGraw-Hill, New York.
- Stramska, M., Stramski, D., Mitchell, B.G., Mobley, C.D. 2000. Estimation of the absorption and backscattering coefficients from in-water radiometric measurements. *Limnol. Oceanogr.* 45: 628–641.
- Toole, D.A., Siegel, D.A., Menzies, D.W., Neumann, M.J., Smith, R.C. 2000. Remote-sensing reflectance determinations in the coastal ocean environment: impact of instrumental characteristics and environmental variability. *Appl. Opt.* 39: 456–469.
- Twardowski, M.S., Boss, E., Sullivan, J.M., Donaghay, P.L. 2004. Modeling the spectral shape of absorption by chromophoric dissolved organic matter. *Mar. Chem.* 89: 69–88.
- Vähätalo, A.V., Wetzel, R.G., Paerl, H.W. 2005. Light absorption by phytoplankton and chromophoric dissolved organic matter in the drainage basin and estuary of the Neuse River, North Carolina (U.S.A.). *Freshwater Biol.* 50: 477–493.
- van de Hulst, H.C. 1980. Multiple Light Scattering. Vols. 1 and 2. Academic Press, New York.
- Welshmeyer, N.A. 1994. Fluorometric analysis of chlorophyll a in the presence of chlorophyll b and pheopigments. *Limnol. Oceanogr.* 39: 1985–1992.
- Yacobi, Y.Z., Gitelson, A.A. 2000. Simultaneous remote measurement of chlorophyll and total seston in productive inland waters. *Verhandlungen des Internationalen Verein Limnologie* 27: 2983–2986.
- Zaneveld, J.R.V. 1995. A theoretical derivation of the dependence of the remotely sensed reflectance of the ocean on the inherent optical properties. *J. Geophys. Res.* 100: 13,135–14,142.
- Zhang, Z., Voss, K.J. 2005. Comparisons of bidirectional reflectance distribution function measurements on prepared particulate surfaces and radiative-transfer models. *Appl. Opt.* 44: 597–610.